Mon. Not. R. Astron. Soc. **000**, 1–18 (2006) Printed 9 October 2018 (MN LATEX style file v2.2)

The first year of SN 2004dj in NGC 2403⋆

J. Vinkó[1]†, K. Takáts[1], K. Sárneczky[1], Gy. M. Szabó[2], Sz. Mészáros[1,5], R. Csorvási[1],T. Szalai[1], A. Gáspár[1], A. Pál[3], Sz. Csizmadia[4], A. Kóspál[4], M. Rácz[4], M. Kun[4], B. Csák[1,5], G. Fűrész[4,5], H. DeBond[6], J. Grunhut[6], J. Thomson[6], S. Mochnacki[6], T. Koktay[6]

[1] *Dept. of Optics & Quantum Electronics, University of Szeged, Hungary*
[2] *Dept. of Experimental Physics, University of Szeged, Hungary*
[3] *Dept. of Astronomy, ELTE University, Budapest, Hungary*
[4] *Konkoly Observatory of Hungarian Academy of Sciences, Budapest, Hungary*
[5] *Harvard-Smithsonian Center for Astrophysics, Cambridge MA, USA*
[6] *David Dunlap Observatory, University of Toronto, Richmond Hill ON, Canada*

Accepted . Received ; in original form

ABSTRACT

New $BVRI$ photometry and optical spectroscopy of the Type IIp supernova 2004dj in NGC 2403, obtained during the first year since discovery, are presented. The progenitor cluster, Sandage 96, is also detected on pre-explosion frames. The light curve indicates that the explosion occured about 30 days before discovery, and the plateau phase lasted about $+110 \pm 20$ days after that. The plateau-phase spectra have been modelled with the $SYNOW$ spectral synthesis code using H, Na I, Ti II, Sc II, Fe II and Ba II lines. The SN distance is inferred from the Expanding Photosphere Method (EPM) and the Standard Candle Method (SCM) applicable for SNe IIp. They resulted in distances that are consistent with each other as well as earlier Cepheid- and Tully-Fisher distances. The average distance, $D = 3.47 \pm 0.29$ Mpc is proposed for SN 2004dj and NGC 2403. The nickel mass produced by the explosion is estimated as $\sim 0.02 \pm 0.01\ M_{\odot}$. The SED of the progenitor cluster is reanalysed by fitting population synthesis models to our observed $BVRI$ data supplemented by U and JKH magnitudes from the literature. The χ^2-minimization revealed a possible "young" solution with cluster age $T_{cl} = 8$ Myr, and an "old" solution with $T_{cl} = 20$ - 30 Myr. The "young" solution would imply a progenitor mass $M > 20\ M_{\odot}$, which is higher than the previously detected progenitor masses for Type II SNe.

Key words: stars: evolution – supernovae: individual (SN 2004dj) – galaxies: individual (NGC 2403)

1 INTRODUCTION

Type II supernovae (SNe) emerge from shock-driven explosion of massive ($M > 8\ M_{\odot}$) stars initiated by core collapse (Woosley & Weaver 1986; Nadyozhin 2003). In particular, plateau Type II SNe (SNe IIp) result from core collapse of supergiants that have massive hydrogen-rich envelope. The light curves of SNe IIp are characterized by a constant luminosity plateau lasting about 80 - 120 days after explosion (Nadyozhin 2003). Recently, the progenitors of a few SNe IIp have been directly identified on pre-explosion images (Maund & Smartt 2005; Van Dyk et al. 2003; Li et al. 2005a; Maund, Smartt & Danziger 2005; Li et al. 2005b), revealing that these are $8 - 15\ M_{\odot}$ supergiants, close to the low-mass theoretical limit of the core collapse process.

SN 2004dj in NGC 2403 is an outstanding SN discovered by Itagaki (Nakano et al. 2004) on July 31, 2004 (JD 2453218), because it is one of the brightest and closest supernova observed ever. Based on its first optical spectrum (Patat et al. 2004) SN 2004dj was quickly classified as a "normal" Type IIp event. Unfortunately, it was discovered during the plateau phase (~ 1 month after explosion), thus, the maximum of the light curve could not be covered. Due to its proximity ($D \sim 3.1$ Mpc) (Freedman et al. 2001), SN 2004dj was also detected in radio (Stockdale et al. 2004; Beswick et al. 2005), infrared (Sugerman & Van Dyk 2005;

⋆ Based on observations obtained at David Dunlap Observatory (Canada), F.L.Whipple Observatory (USA), Konkoly Observatory and Szeged Observatory (Hungary)

† E-mail:vinko@physx.u-szeged.hu

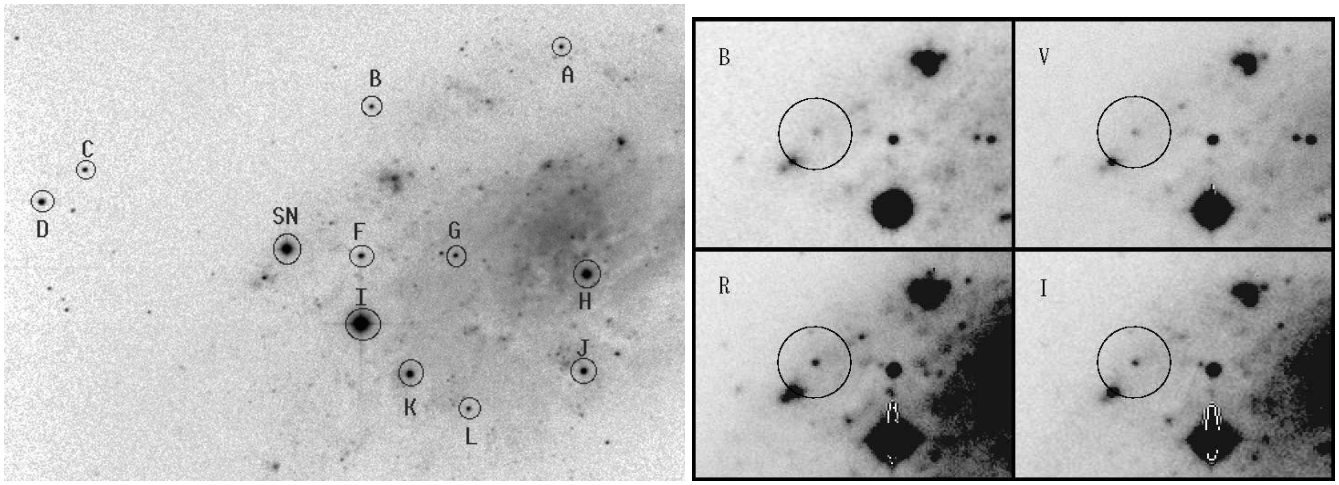

Figure 1. Left: The field of SN 2004dj observed with the Princeton VersArray 1300B CCD on the 1m RCC telescope at Konkoly Obs. The field of view shown is about 7x5 arcmins. North is up and East is to the left. The local comparison stars and the SN are labelled. The standard magnitudes of the comparison stars are listed in Table 2. Right: The detection of the progenitor cluster Sandage 96 on archival frames taken with the 60/90 cm Schmidt telescope and Photometrics CCD at Konkoly Obs. on 11th Jan. 2002. The applied filter is indicated on the upper left corner on each frame.

Kotak et al. 2005) and X-ray bands (Pooley & Lewin 2004). R-band optical photometry and high-resolution $H\alpha$ spectroscopy obtained during the plateau phase was published by Korcakova et al. (2005). Chugai et al. (2005) presented BVR light curve and full optical spectra in the nebular phase. They estimated the amount of ^{56}Ni as $\sim 0.02\ M_{\odot}$, and pointed out an asymmetric, bipolar distribution of the ejected nickel from modeling the nebular $H\alpha$ profile. The optical light curve observed in the BATC (intermediate-band) system was also studied by Zhang et al. (2005). They concluded that SN 2004dj was a typical SN IIp that ejected a $\sim 10\ M_{\odot}$ envelope and synthesized $\sim 0.02\ M_{\odot}$ of radioactive nickel.

Particular interest was paid on the association of SN 2004dj with the compact cluster Sandage 96 which is thought to be the host of the progenitor star (Yamaoka et al. 2004). Maíz-Apellániz et al. (2004) and Wang et al. (2005) analysed the spectral energy distribution (SED) of Sandage 96 (based on archival CCD photometry), and concluded that S96 is indeed a compact cluster with age of $\sim 14 - 20$ Myr and total stellar mass of $\sim 10^4 - 10^5\ M_{\odot}$ (the uncertainty is due to the different reddening determination). From population synthesis, the initial mass of the progenitor star of SN 2004dj was estimated as $12 - 15\ M_{\odot}$, which is in the upper part of the mass range of other SNe IIp progenitors (see above).

In this paper we present time-resolved optical photometry and spectroscopy of SN 2004dj covering its first year after discovery. Our primary goal is to derive a reasonable distance to this SN and its host galaxy NGC 2403 by using all available information. The new observational data are presented in Section 2 and 3. In Section 4 we apply a variant of the Expanding Photosphere Method (EPM) and the SNe IIp Standard Candle Method (SCM) for distance determination, and critically compare the results with other distance estimates of the host galaxy. Based on the improved distance, we estimate some of the physical properties of SN 2004dj and S96 in Section 5. Finally, Section 6 summarizes our results.

2 OBSERVATIONS

2.1 Photometry

The photometric data were collected with four telescopes, whose basic parameters are summarized in Table 1. All observations were made through Johnson-Cousins $BVRI$ filters. The brightness of the SN was tied to local comparison stars, whose magnitudes were calibrated via Stetson's standard field of NGC 7790, when the sky was photometric. These local comparison stars are shown in Fig. 1.

The reduction of the CCD frames was performed in *IRAF* following the standard procedure: bias/dark subtraction and flat field division, The photometry of the reduced frames was computed by two methods. First, the instrumental magnitudes were derived via aperture photometry. The aperture radius was set as 2×FWHM of the stellar images. The local background was determined in an annulus with inner radius and width of 3×FWHM and 2×FWHM, respectively. Because of the galaxy contamination on the SN and several other local calibrator stars, the background flux around each star has been determined with the built-in *centroid* algorithm that is expected to give the best estimate on quickly variable background. In order to test this result, the background level was also calculated with the *mode* algorithm (3×median - 2×mean), after eliminating the outliers that deviated more than 3σ from the mean value. No significant difference was found between the two background levels, suggesting that the background determination around the selected objects is robust.

The stellar magnitudes coming from the aperture photometry were checked with the results of simultaneous PSF-photometry. This was done only for the Konkoly Schmidt telescope frames, where the larger field of view contained 25 - 30 bright stars, thus, reliable PSF could be determined. This comparison is shown in Fig. 2, where the aperture minus PSF magnitudes are plotted against the V magnitude. It can be seen that most of the magnitudes of the two photometric methods agree well within ±0.05 mag. A few out-

Table 1. Basic data of telescopes used for photometric observations. The columns contain the followings: code, observatory, diameter of telescope, manufacturer of CCD, size of CCD in pixels, readout noise in electrons, pixel scale in arcseconds, field of view on the CCD in arcminutes and typical FWHM of stellar PSFs in arcseconds. Note that the CCD at Szeged Observatory was used with 2x2 binning.

Code	Observatory	Telescope	CCD	Pixels	RON (e^-)	Scale (")	FOV (')	FWHM (")
A	Konkoly	60/90 cm Schmidt	Photometrics	1024x1536	14	1.00	17x25.5	3.3
B	Konkoly	100 cm RCC	Princeton VersArray	1340x1300	10?	0.30	6.7x6.5	3.0
C	Szeged	40 cm Cass	SBIG ST-9E	512x512	13	0.70	6x6	3.8
D	FLWO	120 cm	Minicam	4800x4800	7.6	0.30	24x24	1.2

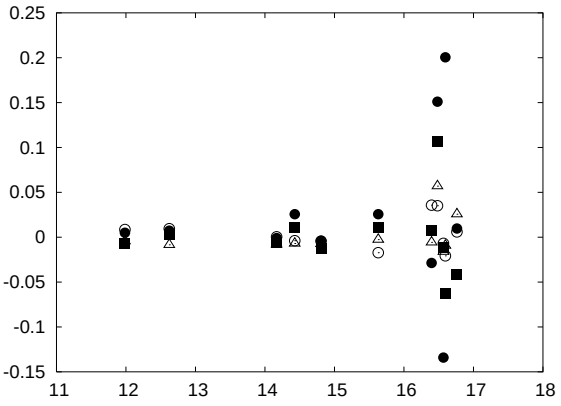

Figure 2. Difference of the magnitudes obtained from aperture- and PSF-photometry against the V magnitude. The symbols denote the filters as follows: filled circles - B, filled squares - V, open circles - R, open triangles - I filter.

liers correspond to the faintest stars in the B band. It is concluded that the results of the aperture photometry with the parameters given above are in accord with the PSF-magnitudes, therefore, the systematic error caused by the photometric method is negligible with respect to the photon/detector noise and errors of the standard transformation.

The host galaxy NGC 2403 was also observed in $BVRI$ bands with the Schmidt telescope at Konkoly Observatory during the course of our nearby galaxy survey programme[1] (Sárneczky et al. 2005) on 23 December 2001 and 11 January 2002. The progenitor cluster Sandage 96 is clearly present on these frames (Fig. 1 right panel). Using the same set of comparison stars, the magnitudes of S96 were computed in the same way as described above. The results are in the last row of Table 2. Our magnitudes are in very good agreement with those presented by Maíz-Apellániz et al. (2004). Because most of the light of the progenitor cluster is still present after the SN explosion, the measured magnitudes of SN 2004dj have been corrected for the light of the progenitor in the following way: the magnitudes of the progenitor as well as those for the SN plus progenitor have been converted into fluxes, then the progenitor fluxes have been subtracted from the SN+progenitor fluxes. The resulting fluxes, expected to be due to only the SN, were transformed back into magnitudes.

In order to further test the reliability of the back-

[1] http://astro.u-szeged.hu/~sn

Table 2. Standard magnitudes of local comparison stars. Errors are given in parentheses. See Fig. 1 for object identification. The last row lists our measurements of the progenitor cluster Sandage 96.

Star	V	$B-V$	$V-R$	$V-I$
A	16.60(0.05)	0.71(0.10)	0.42(0.06)	0.77(0.05)
B	16.80(0.07)	1.57(0.09)	0.97(0.05)	1.84(0.05)
C	16.34(0.06)	0.89(0.07)	0.57(0.04)	0.97(0.03)
D	14.81(0.04)	0.76(0.02)	0.45(0.02)	0.78(0.02)
F	15.61(0.05)	0.95(0.05)	0.58(0.05)	0.97(0.03)
G	16.42(0.05)	0.90(0.06)	0.53(0.04)	0.93(0.04)
H	12.61(0.03)	0.98(0.04)	0.56(0.03)	1.00(0.02)
I	10.06(0.03)	0.56(0.02)	0.38(0.02)	0.64(0.02)
J	14.46(0.04)	0.70(0.04)	0.43(0.03)	0.78(0.02)
K	14.20(0.04)	0.74(0.04)	0.45(0.03)	0.78(0.02)
L	16.66(0.05)	0.88(0.09)	0.54(0.06)	0.92(0.06)
S96	17.85(0.05)	0.40(0.07)	0.33(0.06)	0.79(0.05)

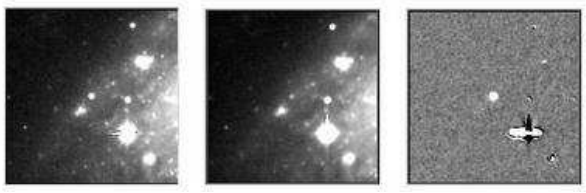

Figure 3. Results of the image subtraction method illustrated with the R frames obtained on May 5, 2005. Left panel: the broadened object frame after convolving with the kernel produced by *psfmatch*. Middle panel: the template frame scaled to the light level of the object frame. Right panel: the difference between the two images. The galaxy and the unsaturated stars have been removed.

ground subtraction and the correction for the progenitor, the Konkoly Schmidt frames were also analysed using the image subtraction method. This was also done with built-in *IRAF* tasks. Three epochs have been selected: Aug.8, 2004 (+39 days after explosion), Nov.02, 2004 (+125 days) and May 13, 2005 (+317 days), when the SN was in the middle of the plateau phase, during the transition phase and in the nebular phase, respectively. The template frames containing the progenitor have been subtracted from the $BVRI$ frames obtained on these epochs with the Schmidt telescope in the following way. First, the images have been registered with the *geomap*, *geotran* and *imalign* tasks. Second, the stellar PSFs on the object and template frames have been matched using the *psfmatch* task. Because the PSFs of the template frames were broader than those of the object frames, the lat-

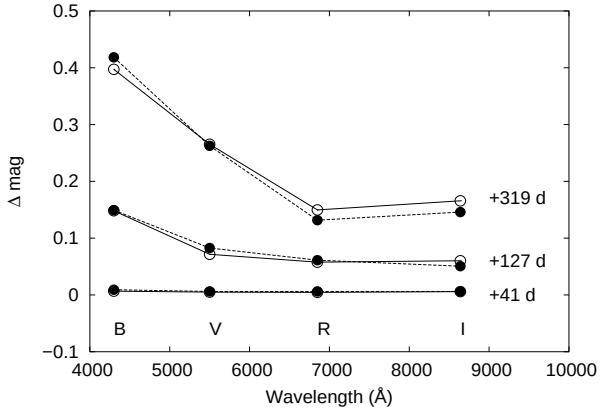

Figure 4. Magnitude corrections due to the progenitor cluster computed with *i*) direct aperture photometry of the SN and template frames (filled circles) and *ii*) image subtraction method (open crcles) as a function of wavelength. The phase of the observation is labelled on the right. The magnitude corrections from the two methods agree within 0.02 mag, even at the last epoch, when the SN was the faintest on our frames.

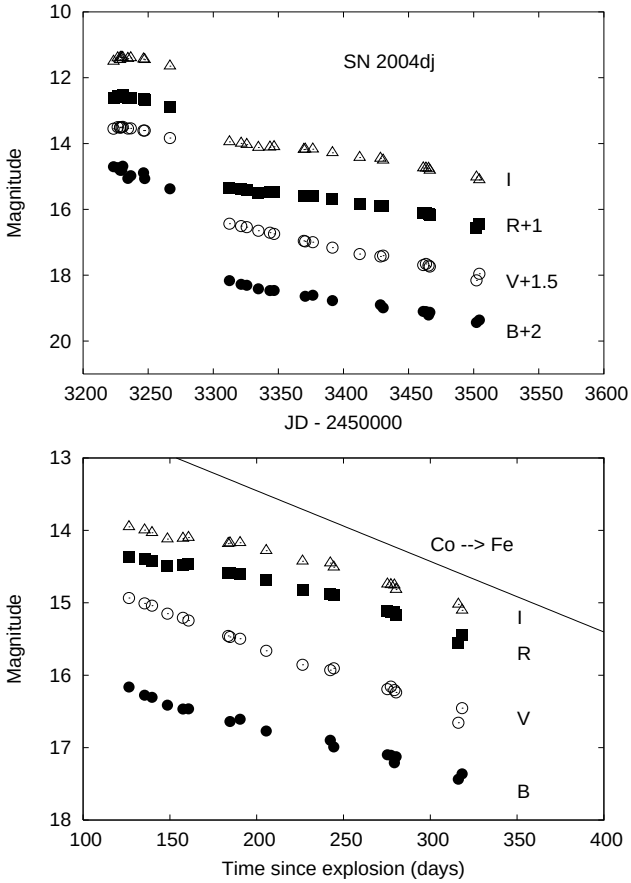

Figure 5. Top panel: Light curve of SN 2004dj in $BVRI$ bands. The curves have been shifted vertically for better visibility with the amount indicated in the legend on the right. Bottom panel: The light curve during the early tail phase. The line indicates the expected slope of the Co-decay.

ter images have been broadened with the kernel produced by *psfmatch*. Third, the intensities of the comparison stars have been scaled to the same level on both frames with the task *linmatch*. Fourth, the scaled template frames have been removed from the broadened object frames to produce the subtracted images. The result of this procedure is illustrated in Fig.3. It is seen that the galaxy and the unsaturated stars have been nicely removed by the image subtraction, leaving a well-defined object (the SN) on a flat background. Then, the aperture photometry have been computed again, now measuring the comparison stars on the broadened object frames, and the SN on the subtracted frames. The SN magnitudes obtained this way were compared with the results of the first method, i.e. that were computed directly on the object frames and corrected for the progenitor magnitudes (see above). Fig.4 shows the difference between the uncorrected and progenitor-corrected SN magnitudes in the case of direct aperture photometry (filled circles), and the difference between the SN magnitudes measured before and after the template subtraction (open circles), as a function of wavelength, for the three epochs considered. It is visible that the corrections coming from the direct photometry do agree within 0.02 mag with those from the image subtraction method, even at the last epoch when the SN was the faintest on our frames. This also means that the galaxy contamination could also be effectively removed with the selected aperture/annulus combination in the first method. Note that this good agreement is partly due to the fact that the object and template frames have been made with the same instrument. The image subtraction method is expected to perform less well for those SN frames that have been made with other telescopes. Moreover, the digital image subtraction always increases the noise on the difference image, resulting in slightly higher uncertainties. Therefore, it is concluded that the light of the progenitor cluster can be reliably removed from the SN magnitudes obtained with direct aperture photometry of the object frames (containing the galaxy and the SN) using the progenitor magnitudes listed in Table 2. The image subtraction method (that removes the host galaxy and the progenitor pixel-by-pixel) gave essentially the same result for the selected frames. In the followings we use the magnitudes of SN 2004dj computed with the first method and corrected for the progenitor magnitudes in Table 2.

Finally, all photometric data were transformed into the standard Johnson-Cousins system using colour terms determined for each telescope/CCD on photometric nights. The final calibrated and progenitor-corrected magnitudes of SN 2004dj are listed in Table 3. The errors (given in parentheses) reflect the observational noise and the uncertainties of the magnitudes of local comparison stars (see Table 2).

The light curves of SN 2004dj are plotted in Fig. 5. This is a typical Type IIp light curve. During the plateau phase the light level is almost constant in V, R, I bands. There is a slow decrease in B, which would be even stronger in the U band. It is generally accepted that this plateau phase is due to a hydrogen recombination front that moves inward the expanding H-rich ejecta. Then, following a rapid transition, the SN enters the nebular phase (often referred as the tail phase), where the light variation reflects the radioactive decay of ^{56}Co into ^{56}Fe. The bottom panel of Fig. 5 shows only the radioactive tail with the expected slope of the Co-decay. It is visible that in the early tail phase the slope of the light curve is less than that of the Co-decay in

Table 3. Observed magnitudes of SN 2004dj. The columns contain the followings: date and JD-2450000 of the observations, days relative to the estimated moment of explosion (JD 2453187, see Sect.4), $BVRI$ magnitudes corrected for the magnitudes of S96 (errors are in parentheses) and codes of the applied telescopes. See Table 1 for the telescope codes.

Date	JD-2450000	$t - t_{expl}$	B	V	R	I	Tel.
2004-08-05	3223.4	36	12.70(0.05)	12.05(0.04)	11.61(0.03)	11.50(0.07)	C
2004-08-08	3226.6	39	12.73(0.06)	12.00(0.03)	11.57(0.03)	11.40(0.03)	A
2004-08-10	3228.4	41	–	12.02(0.03)	11.57(0.03)	11.45(0.05)	C
2004-08-10	3228.6	41	12.81(0.05)	12.00(0.03)	11.58(0.03)	11.39(0.03)	A
2004-08-11	3229.6	42	12.81(0.05)	12.01(0.03)	11.58(0.03)	11.39(0.03)	A
2004-08-12	3230.4	43	12.69(0.05)	11.99(0.03)	11.54(0.05)	11.39(0.03)	C
2004-08-16	3234.4	47	13.06(0.07)	12.04(0.05)	11.61(0.03)	11.42(0.03)	C
2004-08-18	3236.6	49	12.98(0.06)	12.04(0.03)	11.61(0.03)	11.40(0.03)	B
2004-08-28	3246.4	59	12.89(0.12)	12.10(0.03)	11.64(0.03)	11.43(0.03)	C
2004-08-29	3247.3	60	13.07(0.06)	12.11(0.03)	11.68(0.03)	11.45(0.03)	C
2004-09-17	3266.7	79	13.38(0.05)	12.33(0.03)	11.88(0.03)	11.65(0.03)	A
2004-11-02	3312.4	125	16.16(0.05)	14.93(0.04)	14.36(0.03)	13.95(0.03)	A
2004-11-11	3321.4	134	16.28(0.05)	15.01(0.04)	14.39(0.03)	13.99(0.03)	A
2004-11-15	3325.7	138	16.31(0.05)	15.04(0.04)	14.43(0.03)	14.03(0.03)	A
2004-11-24	3334.6	147	16.41(0.17)	15.15(0.08)	14.49(0.08)	14.12(0.06)	B
2004-12-04	3343.5	156	16.47(0.05)	15.21(0.04)	14.48(0.04)	14.11(0.03)	B
2004-12-07	3346.7	159	16.47(0.05)	15.24(0.04)	14.46(0.04)	14.10(0.03)	B
2004-12-29	3369.6	182	–	15.46(0.06)	14.58(0.04)	14.18(0.03)	A
2004-12-30	3370.6	183	16.64(0.05)	15.47(0.04)	14.58(0.05)	14.17(0.03)	A
2005-01-05	3376.4	189	16.61(0.05)	15.50(0.04)	14.60(0.05)	14.17(0.03)	A
2005-01-21	3391.5	204	16.77(0.05)	15.66(0.04)	14.68(0.04)	14.28(0.03)	A
2005-02-10	3412.4	225	–	15.86(0.06)	14.83(0.04)	14.43(0.05)	A
2005-02-26	3428.4	241	16.90(0.06)	15.93(0.04)	14.88(0.05)	14.45(0.05)	A
2005-02-28	3430.4	243	16.99(0.06)	15.90(0.04)	14.89(0.04)	14.51(0.03)	A
2005-03-31	3461.3	274	17.10(0.07)	16.19(0.05)	15.12(0.04)	14.74(0.04)	A
2005-04-02	3463.3	276	17.11(0.07)	16.16(0.05)	15.12(0.04)	14.75(0.04)	A
2005-04-04	3465.3	278	17.21(0.07)	16.21(0.05)	15.13(0.04)	14.76(0.04)	A
2005-04-05	3466.3	279	17.13(0.08)	16.24(0.05)	15.17(0.04)	14.82(0.04)	A
2005-05-12	3502.1	315	17.44(0.10)	16.66(0.05)	15.55(0.04)	15.02(0.04)	D
2005-05-13	3504.3	317	17.36(0.10)	16.46(0.05)	15.44(0.04)	15.10(0.04)	A

R and I. The decline rate in these bands is 0.6 mag/(100 days) compared with the 0.98 mag/(100 days) rate of the Co-decay. On the other hand, the B and V light curve declines with 0.8 mag/(100 days) which is close to the expected rate. Similar phenomenon was found by Zhang et al. (2005) from their intermediate-band light curves: in the $\lambda\lambda 6600 - 8500$ Å wavelength regime the decline rates are much less than the Co-rate. Since the R and I bands are dominated by the $H\alpha$ and Ca-triplet emission lines, which can be particularly strong at the beginning of the tail phase, it is probable that the reduced decline rate in these bands reflects the contribution of these lines to the thermal radiation powered by the trapping of gamma-rays and positrons from the Co-decay.

Chugai et al. (2005) also presented a tail light curve of SN 2004dj obtained through Johnson-Cousins B, V and R filters. Comparing their published photometry with ours presented here, the light curve slopes in different bands are consistent. However, there is a general, systematic offset of 0.3 - 0.4 mag in all bands in the sense that the Chugai et al. magnitudes are systematically brighter. Both sets of light curves have been transformed to the standard system, although there is no star in common in the two groups of local calibrators. Since Chugai et al. (2005) do not mention whether they had corrected their data for the progenitor light, it is probable that this difference is partly due to the presence of the progenitor light in their magnitudes. But it is interesting that if we do not correct our data for the progenitor, the offset is still present, although with a reduced amount (Chugai et al.'s data are still brighter by ~ 0.2 mag). At present, it is not clear what is the cause of this systematic offset, but note that the standard transformation of SN magnitudes obtained with different telescope/CCD/filter combinations are always uncertain at the level of ~ 0.1 mag (Suntzeff 2000) due to the nonstellar SED of the SN, especially during the nebular phase. This effect may easily be responsible for most of the remaining offset.

2.1.1 Comparison with other SNe Type IIp

It is interesting to compare the light curve of SN 2004dj with those of other Type IIp SNe, although it is known that SNe IIp light curves are quite heterogenious. Recently Hamuy & Pinto (2002) and Hamuy (2005) showed that there is a correlation between the absolute magnitudes in the middle of the plateau and the photospheric radial velocity at the same epoch, which partly explains the observed differences in the light curves of different SNe IIp.

Chugai et al. (2005) compared SN 2004dj with SN 1999gi, another well-observed Type IIp SN. Based on the V light curve (supplemented by amateur observations) and an estimated explosion date JD 2453170, they concluded that the two light curves are very similar. Zhang et al.

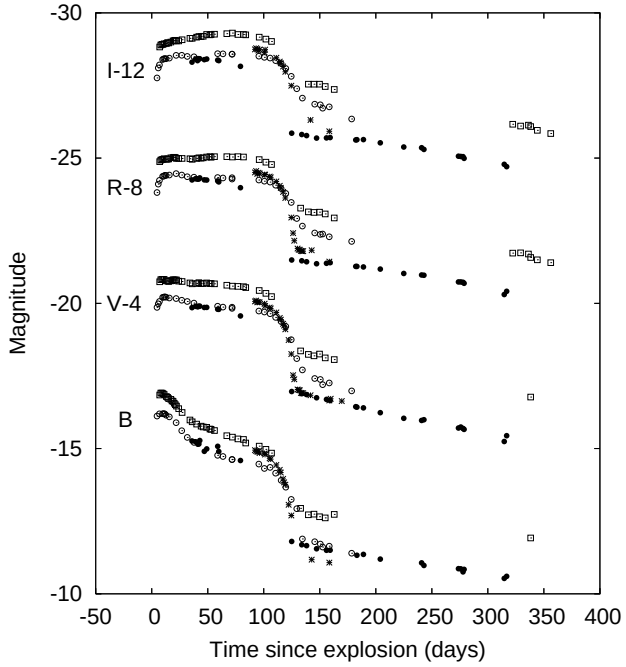

Figure 6. Comparison of the light curves of SN 2004dj (filled circles), SN 1999gi (open circles), SN 1999em (open squares) and SN 2003gd (asterisks). The magnitudes have been corrected for reddening and distance listed in Table 4. The curves have been shifted vertically for better visibility (the amount of the applied magnitude shift is indicated on the left-hand side of each curve

.

(2005) did the same but using the data of SN 1999em for comparison. Based on the assumption that the two light curves should be similar, they estimated the moment of explosion as JD 2453167 ± 21, which was nearly the same as Chugai et al. (2005) determined.

We compared our new light curve (Fig.5 and Table 3) with the published magnitudes of SN 1999em (Leonard et al. 2002a) , SN 1999gi (Leonard et al. 2002b) and SN 2003gd (Hendry et al. 2005) To do this, all data were corrected for reddening and distance modulus, collected from references listed in Table 4. For SN 1999em we have used the distance derived recently by Dessart & Hillier (2005b), which is in good agreement with the Cepheid-based distance of its host galaxy. For SN 2004dj we have applied our preferred values of $E(B-V) = 0.07$ mag, $T_{expl} = 2453187$ and $D = 3.47$ Mpc (see Section 4). The absolute magnitudes for each SN are plotted together in Fig.6.

From Fig.6 it is visible that the absolute light level of SN 2004dj is similar to that of SN 1999gi during the plateau phase, but different from those of SNe 1999em and 2003gd. This difference may be due to different nickel masses for these SNe. However, as it will be discussed in Section 2.2, the spectra and the expansion velocities are quite similar for SN 2004dj and SN 1999em in the middle of the plateau phase, that would suggest similar plateau magnitudes (Hamuy & Pinto 2002). It seems that the plateau phase of SN 2004dj ended slightly early relative to 99em and 99gi. Comparing our data with the R light curve of Korcakova et al. (2005), we estimate the starting date of the transition into the nebular phase as $t = +80 \pm 20$ days (the uncertainty is due to both the poor sampling of the light curves around this epoch and the uncertainty of the explosion date). The inflection time (Elmhamdi et al. 2003a) for SN 2004dj is estimated as $t_i = +110 \pm 20$ days, which is slightly earlier than that for SN 1999em ($+120 \pm 4$ days) and SN 1999gi ($+125 \pm 3$ days), but this is not a significant difference because of the relatively high uncertainty of the explosion date of SN 2004dj.

Table 4. Light curve parameters of Type IIp SNe used for comparison.

SN	E(B-V) (mag)	t_{expl} (JD-2450000)	D (Mpc)	Ref.
1999em	0.10	1475	11.5	1,3
1999gi	0.22	1518	10.8	2
2003gd	0.14	2717	9.3	4
2004dj	0.07	3187	3.47	5

References - (1) Leonard et al. (2002a); (2) Leonard et al. (2002b); (3) Dessart & Hillier (2005b); (4) Hendry et al. (2005); (5) present paper

In the nebular phase, SN 2004dj has the faintest light level among these four SNe, except in B where SN 2003gd is slightly fainter. The faintness of SN 2004dj is increasing toward longer wavelengths. In this phase SN 2004dj is more similar to SN 2003gd (Van Dyk et al. 2003; Hendry et al. 2005) than the other two SNe. Elmhamdi et al. (2003a) found that the tail light level of SNe IIp correlate well with the plateau magnitude in V. From Fig. 6 it is suspected that this correlation is actually weak in V, and probably not valid at all in R and I.

Since SNe IIp tail light curves are powered by radiactive decay of ^{56}Co - ^{56}Fe, different brightness probably reflects the difference in the amount of the synthesized iron-peak elements, particularly ^{56}Ni (Nadyozhin 2003; Elmhamdi et al. 2003a). From hydrodynamic models Nadyozhin (2003) pointed out that the middle-plateau absolute magnitude M_V is proportional to the plateau duration Δt_p, the expansion velocity in the middle of the plateau and the explosion energy (see Eq.1 of Nadyozhin (2003)). Thus, from the shape of the light curve alone, we suspect that SN 2004dj had similar explosion energy and nickel mass than those of SN 1999gi, but less than those of SN 1999em. We will examine this question more quantitatively in Section 5.

2.1.2 Reddening

Reddening is the key parameter when photometry is used to derive physical parameters. From the literature, the reddening of SN 2004dj is controversial. Patat et al. (2004) reported the identification of interstellar Na D (from an unresolved absorption trough) in the very first spectrum of SN 2004dj, from which they deduced $E(B-V)_{total} = 0.18$ mag. 1 day later Guenther & Klose (2004) stated that with high-resolution echelle spectroscopy they resolved the Na D lines in the host galaxy NGC 2403. They revealed the contribution of the host galaxy to the reddening of SN 2004dj as $E(B-V)_{host} = 0.026$ mag. Since the galactic component is only $E(B-V)_{gal} = 0.04$ mag (Schlegel et al. 1998), this

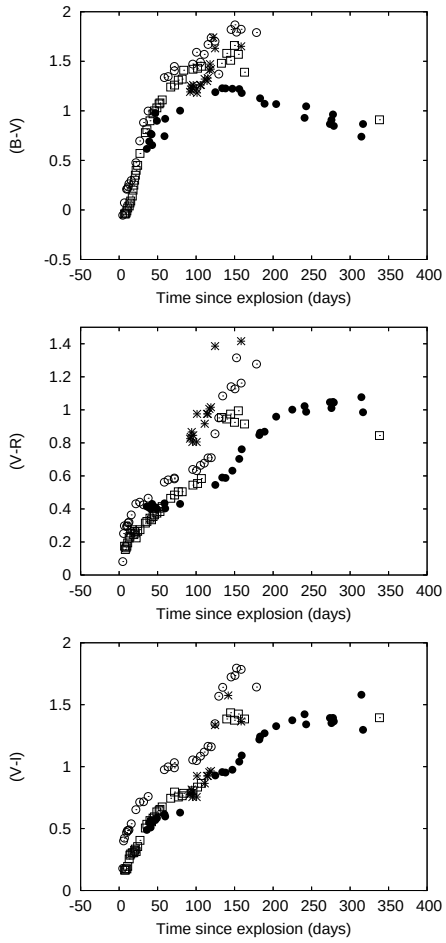

Figure 7. The colour curves of SNe 2004dj, 1999em, 1999gi and 2003gd corrected for galactic reddening (see text). The symbols are the same as in Fig. 6.

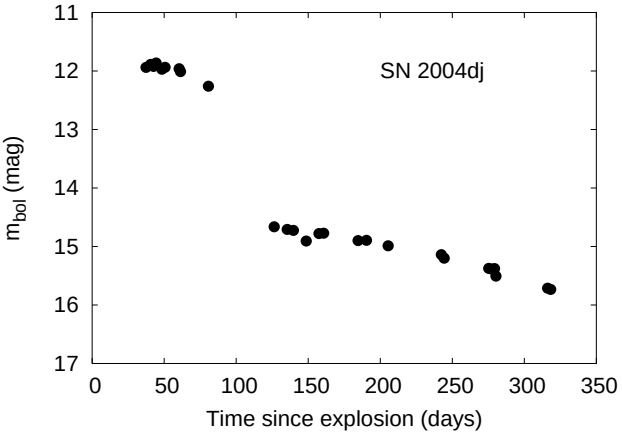

Figure 8. *UVOIR* bolometric magnitudes of SN 2004dj, corrected for reddening ($E(B-V) = 0.07$ mag). The bolometric fluxes (Table 5) have been transformed into magnitudes via Eq.1.

indicates significantly less total reddening ($E(B-V)_{total} = 0.066$) than Patat et al. (2004) estimated.

Reddening has also been determined indirectly from population synthesis models of the progenitor cluster S96. Fitting cluster SEDS to archival optical and near-IR ($UBVRIJHK$) photometric data of S96, Maíz-Apellániz et al. (2004) derived $E(B-V)_{total} \approx 0.13 \pm 0.03$ mag. This value is between the two direct spectral measurement mentioned above, being definitely in better agreement with the result of Patat et al. (2004). On the other hand, Wang et al. (2005) have applied essentially the same technique using their own O-IR photometric data (through intermediate-band filters, providing better wavelength coverage in the optical) on S96. They have obtained $E(B-V)_{total} = 0.35 \pm 0.05$ mag, arguing that this value provides a better fit of the calculated SEDs. Zhang et al. (2005) also derived $E(B-V)_{total} = 0.33 \pm 0.11$ mag from the reanalysis of the EW of the interstellar Na D trough reported by Patat et al. (2004). It is clear that the present estimates of the extragalactic reddening toward SN 2004dj range from an almost negligible value (Guenther & Klose 2004) to significant in-host extinction (Wang et al. 2005; Zhang et al. 2005).

Comparing our observed colour curves of SN 2004dj with those of SNe 1999em, 1999gi and 2003gd some constraints can be determined on the upper or lower limits of reddening (Leonard et al. 2002b). Fig. 7 shows the $B-V$, $V-R$ and $V-I$ curves of these four SNe IIp corrected for the galactic reddening (the following values were adopted from NED: $E(B-V)_{gal} = 0.04,\ 0.04,\ 0.017$ and 0.069 mag for SNe 2004dj, 1999em, 1999gi and 2003gd, respectively). SN 2004dj has the bluest colours among these SNe, especially in the transition and the nebular phase. Since SNe 1999em, 1999gi and 2003gd suffered only moderate reddening in their hosts (see Table 4), the bluer colour of SN 2004dj means that $E(B-V)_{total} > 0.1$ mag is less probable. Thus, the observed colour curves favour lower reddening, such as that determined by Guenther & Klose (2004). This may also be preferred, because this is the only one that is based on *direct* measurement of the resolved interstellar Na D lines within the host galaxy. Note that Chugai et al. (2005) also selected $E(B-V)_{total} = 0.062$ mag for SN 2004dj based on their observed colour indices, but they attributed it entirely to galactic extinction.

In the followings we adopt $E(B-V)_{total} = 0.07 \pm 0.1$ mag as the most probable total (galactic plus host) reddening of SN 2004dj. Its uncertainty is estimated from the scattering of the spectroscopic measurements mentioned above.

2.1.3 The bolometric light curve

The $UVOIR$ bolometric light curve has been calculated from the observed $BVRI$ magnitudes plus extrapolating an assumed (over-)simplified SED to the wavelength bands not covered by the observations. First, the observed magnitudes were corrected for extinction using $E(B-V) = 0.07$ mag (see previous section) and the standard galactic reddening law (Schlegel et al. 1998). $K-$corrections were neglected, because the redshift of the host galaxy is very small, $z = 0.00044$ (NED). The dereddened magnitudes were then transformed to fluxes using the calibration given by Hamuy et al. (2001). The fluxes have been integrated numerically using the effective wavelengths and FWHM values

Table 5. $UVOIR$ bolometric fluxes and magnitudes of SN2004dj.

JD-2450000	$t - t_{expl}$ (days)	f_{bol} (10^{-10} erg/s/cm^2)	m_{bol} (mag)
3223.4	36	4.14	11.94
3226.6	39	4.35	11.89
3228.6	41	4.30	11.90
3229.6	42	4.30	11.90
3230.4	43	4.44	11.87
3234.4	47	4.02	11.97
3236.6	49	4.12	11.95
3246.4	59	4.06	11.97
3247.3	60	3.88	12.02
3266.7	79	3.16	12.24
3312.4	125	0.33	14.68
3321.4	134	0.32	14.74
3325.7	138	0.31	14.77
3334.6	147	0.28	14.86
3343.5	156	0.28	14.86
3346.7	159	0.28	14.86
3370.6	183	0.25	14.97
3376.4	189	0.25	14.97
3391.5	204	0.23	15.08
3428.4	241	0.19	15.26
3430.4	243	0.19	15.31
3461.3	274	0.15	15.53
3463.3	276	0.15	15.53
3465.3	278	0.15	15.56
3466.3	279	0.14	15.59
3502.1	315	0.11	15.86
3504.3	317	0.11	15.86

of the $BVRI$ filters by a simple midpoint rule. The fluxes in the missing UV and IR bands were extraplolated linearly from the B and I fluxes assuming zero flux at 3400 Å and 23000 Å.

This approximation has been tested by integrating the known $BVRI$ magnitudes of Vega and the Sun (Hamuy et al. 2001) and comparing the resulting quasi-bolometric fluxes with the observed ones. The relative error of the bolometric flux calculated in this way turned out to be 9.6 % and 0.6 % (0.11 and 0.001 mag) for the Sun and Vega, respectively. Because during the plateau phase the SED of the SN is similar to stellar photospheres, and the effective temperature in most cases is between the temperature of the Sun ad Vega ($5800 < T_{SN} < 10000$ K), we believe that the uncertainty of our bolometric fluxes due to the approximation applied does not exceed significantly the level of 10 percent at the early phases.

During the nebular phase, the SED of the SN becomes nonstellar, therefore the comparison with stellar flux distributions may be misleading. Fortunately, SN 2004dj was detected with the IRAC and MIPS instruments onboard the Spitzer Space Telescope on four epochs at the beginning of the nebular phase. Kotak et al. (2005) presented the photometry made in 5 channels in the mid-IR regime (from 3.6μ to 24μ). These infrared fluxes were used to test the quality of our quasi-bolometric fluxes in the nebular phase. Assuming negligible reddening in the mid-IR regime, the SED of SN 2004dj was constructed using the IR fluxes obtained on Nov.1, 2004 (Kotak et al. 2005) and our optical fluxes observed on the same epoch (Table 3). The missing near-IR fluxes were estimated by interpolation between the optical and mid-IR fluxes, assuming power-law wavelength dependence. This SED was then integrated along wavelength using the same approximation in the UV boundary as before, but extending the IR boundary up to 8 microns. The result was $0.317 \cdot 10^{-10}$ erg/s/cm^2, comparing with $0.33 \cdot 10^{-11}$ erg/s/cm^2 estimated from the optical data. The relative difference in only 4 percent, which is nearly the same as it was in the photospheric phase. Thus, it is concluded that the approximative, quasi-bolometric fluxes, estimated from $BVRI$ fluxes have about 10 percent uncertainty, both in the plateau and the early nebular phase.

Finally, the bolometric fluxes have been transformed into magnitudes using

$$m_{bol} = -2.5 \log_{10} [f_{bol}] - 11.512 \quad (1)$$

where the zero-point was determined from the solar luminosity and absolute bolometric magnitude ($M_{bol\odot} = +4.72$ mag and $L_\odot = 3.847 \cdot 10^{33}$ erg s^{-1} was used). The bolometric magnitudes are plotted against time in Fig. 8. The slope of the light curve is clearly increasing in the radioactive tail phase (as it was also presented in Fig. 5). At $t \approx +120$ days after explosion the slope is about -0.45 mag/100 days, while around $t \approx +300$ days it increases up to -0.8 mag/100 days which is closer to the expected theoretical value of the Co-decay (-0.98 mag/100 days). We deduce that SN 2004dj entered fully the radioactive nebular phase around +350 - +400 days after explosion. We analyse the bolometric light curve further in Section 4 and 5.

Table 6. Journal of spectroscopic observations. The columns contain the following data: date and JD ($-$ 2450000) of the observations, days relative to the estimated moment of explosion (JD 2453187, see Sect.4.1), central wavelength and airmass.

Date	JD-2450000	Days	λ_c	Airmass
2004-08-17	3234.9	47	5800	1.57
2004-08-20	3237.6	50	5800	2.92
2004-08-22	3239.9	52	5800	1.47
2004-08-25	3242.9	55	5800	1.49
2004-09-03	3251.8	64	5800	1.49
2004-09-04	3252.8	65	5800	1.53
2004-09-06	3254.9	67	5800	1.04
2004-09-22	3270.9	83	5800	1.22
2004-10-02	3281.7	94	5800	1.24
2004-10-03	3282.9	95	5800	2.02
2004-10-05	3284.9	97	5800	2.25
2004-10-06	3285.5	98	5800	1.13
2004-10-07	3286.9	99	5800	1.70
2004-11-14	3324.7	137	5800	1.32

2.2 Spectroscopy

The spectroscopic observations were conducted at David Dunlap Observatory (DDO) with the 74" telescope and the Cassegrain spectrograph. The 100 lines/mm grating was applied giving a 2-pixel-resolution of about 800 at 6000 Å. The journal of spectroscopic observations is presented in Table 6.

The spectra were reduced and calibrated in the usual way using *IRAF*. After bias, flatfield and cosmic-ray corrections, the spectrum was extracted with the

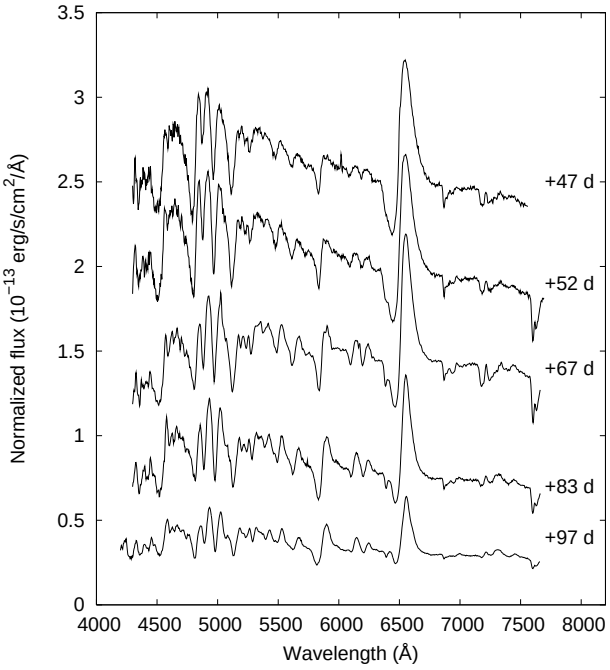

Figure 9. Spectral evolution of SN 2004dj during the plateau and the transition phase. Labels indicate the elapsed time since the estimated date of explosion in days. The spectra have been shifted vertically by $5 \cdot 10^{-14}$ erg/s/cm^2/Å for better visibility.

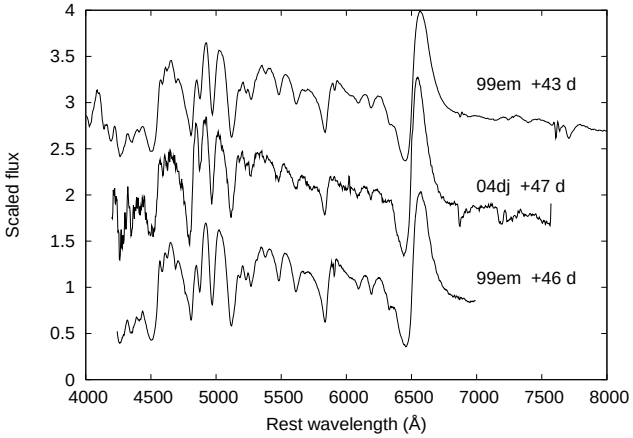

Figure 10. Comparison of the spectra of SN 2004dj (thick line) and SN 1999em (thin line). The time since explosion is labelled. The spectra were dereddened, corrected for redshift of the host galaxy and shifted vertically for better visibility.

noao.twodspec.apall task. The wavelength calibration was done using two exposures of a FeNe spectral lamp made before and after each target observation. For flux calibration, HD 42818 (sp.type A0V, Adelman et al. (1989); Kharitonov et al. (1988)) was observed as a flux standard.

The DDO Cassegrain spectrgraph has a known limitation in obtaining low resolution spectra, because the slit cannot be rotated, therefore the observations cannot be made at the parallactic angle. Due to this technical limitation, the continuum slope of our spectra is certainly affected by the differential atmospheric refraction, especially in the blue. The most distorted spectrum is the one that was taken on 20th August, 2004, when the airmass was nearly 3 (see Table 5). On the other hand, those spectra that were observed between airmasses of 1 and 1.5 are probably less distorted, thus, they may be used for quantitative analysis. Nevertheless, the blue end of all spectra was set as 4300 Å in order to eliminate the most unreliable blue part.

In the following subsections we present and discuss the plateau and nebular spectra of SN 2004dj separately.

2.2.1 Plateau phase

Fig. 9 shows five representative spectra from the 13 ones obtained during the plateau phase. The plateau-phase spectra are typical for Type IIp SNe: dominant hydrogen lines with P Cygni profiles and moderately strong metallic line blends in the blue, superimposed on a continuum that is increasing toward the blue. Since the spectral evolution is slow in this phase, the other spectra are very similar to those plotted in Fig. 9.

The evolution of the spectral features is also similar to other SNe Type IIp. When the ejecta cools, the continuum gets fainter and redder. The emission component of $H\alpha$ becomes stronger, while the strength of $H\beta$ and the other excited Balmer lines decreases. Among the metallic lines, Na D develops a strong P Cygni profile at the end of the plateau phase. Unfortunately, no spectrum earlier than +47 day was available for us, so we could not check the presence of He in the early phases.

Our first spectrum of SN 2004dj was compared with the spectra of SN 1999em (Leonard et al. 2002a) made at similar phases. These comparison spectra were downloaded from the SUSPECT [2] database. Fig. 10 shows that the spectra of the two SNe are very similar. This is slightly in contrast with the difference between the light curves of the two SNe found in Sect.2.1.1.

From the photospheric spectra the radial velocities of the expanding ejecta were estimated from the Dopplershift of the λ5169 Å Fe II line. Recently Dessart & Hillier (2005a) pointed out that this line is a good indicator of the photospheric velocity. This line is also favoured by Hamuy & Pinto (2002) for estimating the expansion velocity in the middle of the plateau phase. The velocities are plotted in Fig. 11 as filled circles. Because our spectra do not cover the plateau phase well, the first radial velocity point was computed from the line positions reported by Patat et al. (2004). Fig. 11 also contains the radial velocities estimated from the minimum of $H\alpha$. As it is expected, the optically thick $H\alpha$ forms at higher atmospheric levels, probing higher ejecta velocities than the photospheric Fe II lines.

The measured radial velocities must be corrected for the motion of the host galaxy and the SN itself within the host (the barycentric motion of the Earth is usually negligible in the case of SNe). This is often done using the redshift of the host galaxy adopted from major databases. In the case of SN 2004dj, the host galaxy, NGC 2403, has a recession velocity of +131 km/s (NED). Moreover, the SN is located

[2] http://bruford.nhn.ou.edu/∼suspect/index1.html

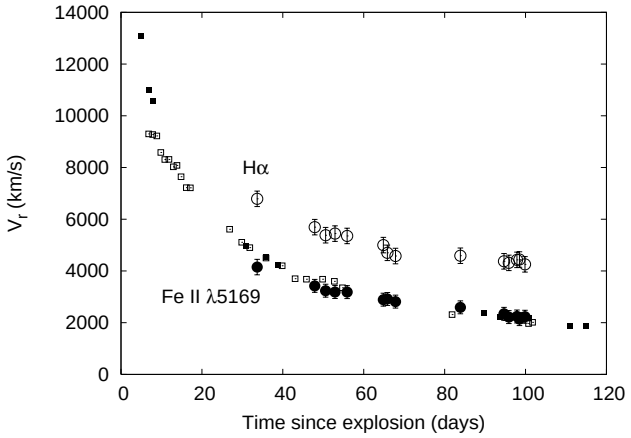

Figure 11. Radial velocities of SN 2004dj. The photospheric velocities (filled circles) have been computed from the Doppler-shift of the λ5169 Fe II line (see text). For comparison, photospheric velocities of SN 1999em (open squares, Leonard et al. (2002a)) and SN 1999gi (filled squares, Leonard et al. (2002b)) are also plotted. The $H\alpha$ velocities of SN 2004dj are shown as open circles.

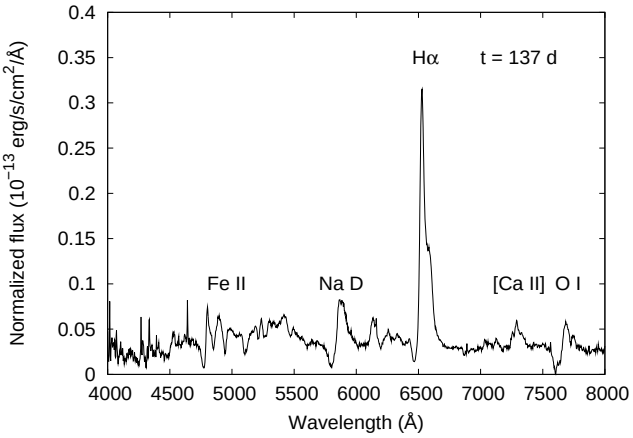

Figure 12. A nebular spectrum of SN 2004dj, +137 days after the explosion.

Table 7. Photospheric radial velocities of SN 2004dj corrected for redshift (+131 km/s) and host galaxy rotation (+90 km/s). The third column lists the average radial velocities calculated from the λ5169 Fe II line. The fourth column contains the velocities based on the minimum of $H\alpha$. Errors are given in parentheses.

JD-2450000	Days	v_r (km/s)	$v_{H\alpha}$ (km/s)
3220.67[1]	33	4150 (300)	6790 (300)
3234.89	47	3423 (250)	5693 (300)
3237.59	50	3236 (250)	5382 (300)
3239.89	52	3184 (250)	5444 (300)
3242.89	55	3183 (250)	5353 (300)
3251.86	64	2888 (250)	5001 (300)
3252.85	65	2917 (250)	4700 (300)
3254.86	67	2813 (250)	4577 (300)
3270.90	83	2592 (250)	4589 (300)
3281.67	94	2342 (250)	4373 (300)
3282.87	95	2214 (250)	4312 (300)
3284.87	97	2239 (250)	4428 (300)
3285.49	98	2136 (250)	4443 (300)
3286.86	99	2230 (250)	4256 (300)

[1] from Patat et al. (2004)

close the outer end of a spiral arm, thus, its radial velocity is expected to differ from the systemic velocity of the whole galaxy. Indeed, Fraternali et al. (2001) recently mapped the kinematics of NGC 2403 via H I emission. It is visible in their Fig. 1 that the area around SN 2004dj is on the receding side of the galaxy. The excess velocity was estimated to be +90 km/s, thus, the total radial velocity of the barycenter of SN 2004dj was set as +221 km/s. The final radial velocities of the SN ejecta were calculated with respect to this value (see Table 7).

2.2.2 Nebular phase

Fig. 12 shows a single spectrum obtained at the beginning of the nebular phase ($t = +137$ days after explosion). The spectrum is dominated by strong $H\alpha$ emission and P Cygni profiles of Na I, O I and Fe II. The forbidden [Ca II] line is also apparent around 7300 Å. Recently Chugai et al. (2005) analysed a more extensive set of nebular spectra of SN 2004dj. They have pointed out significant asymmetry of the $H\alpha$ profile, from which they concluded that the ejection of ^{56}Ni (which is the primary source of $H\alpha$ emission in the nebular phase via radioactive decay) was bipolar inside a spherically symmetric envelope. We do not consider this topic in detail, except noting that our nebular spectrum of SN 2004dj (Fig. 12) do confirm the strong blueward asymmetry of the $H\alpha$ emission profile found by Chugai et al. (2005). So far this phenomenon was reported only in two other SNe, namely SN 1987A (Phillips & Williams 1991) and SN 1999em (Elmhamdi et al. 2003b).

3 SPECTRAL MODELLING

The photospheric spectrum obtained on Aug.17, 2004 (day +47, Table 6) is modelled using the *SYNOW* parametrized spectrum synthesis code (Fisher 2000; Baron et al. 2000; Branch et al. 2003, 2004). This code assumes homologous expansion of the SN ejecta, i.e. $v(r) = r \cdot v_{ph}/R_{ph}$, where r is the radius of a thin shell above the photosphere, $v(r)$ is the velocity of the shell, R_{ph} and v_{ph} is the photospheric radius and the velocity at the photosphere, respectively. Line formation is treated as in the Schuster-Schwarzschild model: the photosphere radiates as a blackbody with temperature T_{bb}, and the lines are formed entirely in the envelope above the photosphere. The line formation is assumed due to pure scattering. This is equivalent to setting the line source function as

$$S(r) \;=\; \frac{I_{ph}}{2}\;\left[1-\sqrt{1-\left(\frac{R_{ph}}{r}\right)^2}\right] \qquad (2)$$

Table 8. Reference line parameters and optical depths of the SYNOW model spectrum shown in Fig. 11. The model has been computed assuming $T_{bb} = T_{exc} = 8000$ K, $v_{ph} = 3400$ kms^{-1} and $\alpha = 6$ (see text). The columns give the following data: name and ionization state of the element, wavelength (in Å), oscillator strength, excitation potential (in eV) and the fitted optical depth for the reference line.

Ion	λ (Å)	log(gf)	χ (eV)	τ_{ref}
H I	6563	0.71	10.21	200
Na I	5890	0.12	0.00	1.1
Sc II	4247	0.32	0.32	1.0
Ti II	4550	-0.45	1.58	8.0
Fe II	5018	-1.40	2.89	4.0
Ba II	4554	0.19	0.00	2.0

where $I_{ph} = B_\lambda(T_{bb})$ is the specific intensity at the photosphere. The optical depth as a function of radius was expressed as a power law:

$$\tau(r) = \tau_0 \left(\frac{r}{R_{ph}}\right)^{-\alpha} \quad (3)$$

In *SYNOW* the fit of the spectral lines is controlled by adjusting the optical depth of a reference line (a strong line in the optical regime) for each element. The depths of other lines are computed via the Boltzmann-equation. The solution of the radiative transfer equation is performed in the Sobolev approximation (Kasen et al. 2002).

Table 8 lists the elements identified in the day +47 spectrum, together with their atomic parameters and fitted reference line optical depths. The model spectrum and the observed one are plotted in Fig. 13. The photospheric temperature was set as $T_{bb} = 8000$ K determined from the slope of the red continuum. The velocity at the photosphere was chosen as $v_{ph} = 3400$ kms^{-1}, which gives $R_{ph} = 922$ Mkm (1324 $R_\odot$) for the radius of the photosphere +47 days after explosion. The optical depth exponent that gives the best description of the observed spectrum was found as $\alpha = 6$.

The elements that could be identified unambigously are H, Na I, Sc II and Fe II. Ti II is assumed to be responsible for the blends below 4800 Å, but other elements (e.g. Ca, Mg, Ni, Co) may also contribute. Ba II is also present, but its contribution is weak and blended by Fe II. Because the overall appearance of the spectrum is very similar to that of SN 1999em (Fig. 10), the more extensive line identification by Leonard et al. (2002a) is probably also valid in this case. Fig. 14 shows the contribution of the elements listed in Table 8 to the spectrum of SN 2004dj.

3.1 The $H\alpha$ profile

It is seen in Fig. 13 that $H\alpha$ cannot be fitted well by *SYNOW*: the absorption is too deep and the emission is too low in the model spectrum. This is a usual situation in modelling a strong line with a pure scattering source function (Branch et al. 2003). It does not necessarily mean the breakdown of the Sobolev approximation, but the source function probably differs from that in Eq.1.

We found that a simple modification of the line source function can sufficiently explain the emission content of $H\alpha$

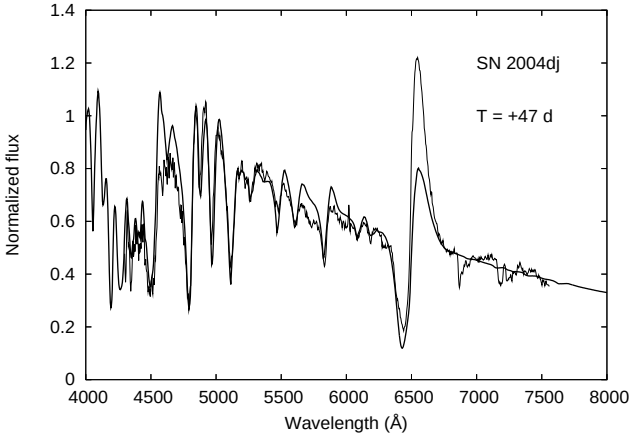

Figure 13. The SYNOW model fit (thick line) and the +47 days observed spectrum (thin line). The model parameters are listed in Table 8.

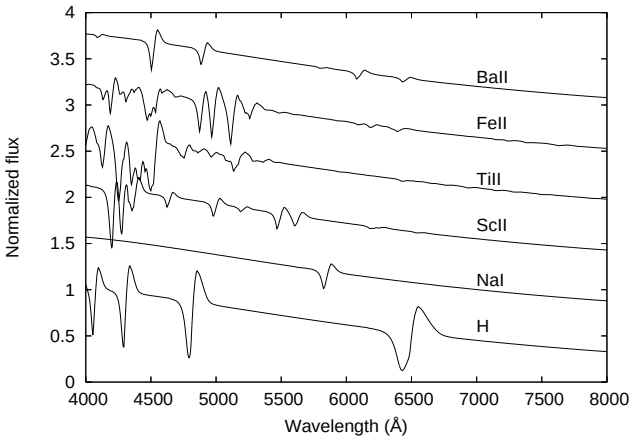

Figure 14. The contribution of chemical elements to the observed spectrum. The labels on the right-hand side indicate the composition. The adopted parameters are the same as in Table 8.

within the Sobolev approximation. Now the source function takes the form

$$S(r) = K\ S_0(r) \quad (4)$$

where $S_0(r)$ is the function given in Eq.1 and K is a constant in r. In fact, K simply scales the photospheric intensity, but the shape of the source function remains the same as the pure scattering one. Fig. 15 shows the line profiles computed with $K = 1$ and 2. The agreement with the observed spectrum is much better when $K = 2$, i.e. the photospheric intensity has an excess with respect to the blackbody intensity at the wavelength of $H\alpha$. Since the photosphere is actually a hydrogen recombination front in SNe IIp, the excess emission can be interpreted as due to the recombination of hydrogen to the $n = 3$ excited state followed by a downward transition to the $n = 2$ state, producing spontaneous emission at the wavelength of $H\alpha$. The exact form of the source function in SNe IIp atmospheres would deserve fur-

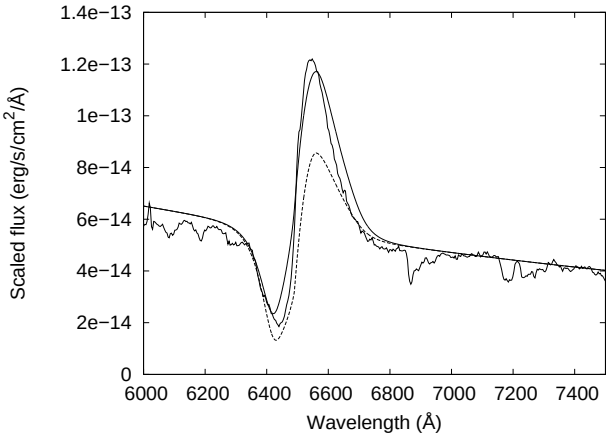

Figure 15. The $H\alpha$ line profile computed with the scaled source function (Eq.4). The continuous line corresponds to $K = 2$, while the dashed line is for $K = 1$. The observed line profile is also shown for comparison (thick line).

ther study. Kasen et al. (2002) presented a technique for determining the source function (as well as the optical depth) as a function of r. We leave this interesting problem for future studies.

4 DISTANCE DETERMINATION

There are a number of methods for determining SNe IIp distances. The Expanding Photosphere Method (EPM) (Kirshner & Kwan 1974; Hamuy et al. 2001; Leonard et al. 2002a,b; Dessart & Hillier 2005a), a variant of the famous Baade-Wesselink method, derives the angular diameter from both photometry and radial velocities, and their comparison yields the distance. The more sophisticated extension of this method is the Spectral Fitting Expanding Atmosphere Method (SEAM) (Baron et al. 1994), which uses a custom-crafted SN model atmosphere and full treatment of hydrodynamics and radiative transfer to fit model spectra to the observed ones. SEAM has been succesfully applied to SNe IIp and other types as well. SEAM stands on more solid physical basis than EPM, but requires much more computing power.

The Standard Candle Method (SCM) (Hamuy & Pinto 2002) relies on the correlation between the absolute magnitude and the radial velocity of the SN ejecta in the middle of the plateau phase. Here the distance can be found by comparing the observed and the calculated absolute magnitudes, like in the case of Cepheids. The so-called "Plateau-Tail Method" (PTM) (Nadyozhin 2003) compares the SN light curve with theoretical models and derive the distance via the model parameters.

In the following we apply EPM and SCM to derive the distance to SN 2004dj, and compare it with distances of the host galaxy found by other methods.

4.1 Expanding Photosphere Method

The methodology of EPM has been recently reviewed and thoroughly discussed by Dessart & Hillier (2005a). They concluded that EPM is best used at early phases, when the SN ejecta is fully ionized and continuum opacity dominates line opacities in the optical. Unfortunately, SN 2004dj could not be observed at such early phases, which makes the application of EPM problematic. Nevertheless, we try to use EPM for the earliest observed data of SN 2004dj and critically compare the results with other distance estimates to minimize the systematic errors caused by the possible failure of the asssumptions of EPM.

Table 9. Quantities derived during the EPM. The columns contain the followings: JD −2450000 of observation, temperatures (in Kelvins), angular sizes (in 10^9 km Mpc^{-1}), and values of θ/v_{ph} (in day Mpc^{-1}).

t	T_{BVI}	T_{VI}	θ_{BVI}	θ_{VI}	$(\theta/v)_{BVI}$	$(\theta/v)_{VI}$
3223.4	7047	10602	3.347	1.700	9.674	4.912
3226.6	6632	9988	3.618	1.967	10.984	5.973
3228.6	6419	9795	3.684	2.033	11.568	6.385
3229.6	6412	9727	3.687	2.062	11.752	6.571
3230.4	6823	9851	3.570	2.043	11.511	6.589
3234.4	5955	9653	3.722	2.023	12.841	6.980
3236.6	6079	9385	3.729	2.163	13.340	7.740

EPM has been applied in the same way as described by Vinkó et al. (2004). The angular radius has been derived from the $UVOIR$ bolometric light curve (Sect.2.1.3) as

$$\theta = \sqrt{\frac{f_{bol}}{\xi^2(T)\sigma T_{eff}^4}} \quad (5)$$

where f_{bol} is the "observed" bolometric flux, T_{eff} is an effective temperature of the diluted blackbody and $\xi(T)$ is the dilution factor (determined from SNe IIp model atmospheres). For each epoch, the effective temperature has been estimated by fitting blackbodies to the dereddened BVI and VI fluxes (the R band has been omitted because of the presence of $H\alpha$ emission).

The dilution factor $\xi(T)$ in Eq.5 comes from model atmospheres. We have adopted the dilution factors derived by Eastman, Schmidt & Kirshner (1996) and parametrized by Hamuy et al. (2001). Recently Dessart & Hillier (2005a) derived new dilution factors that are systematically higher than those of Eastman, Schmidt & Kirshner (1996). The effect of using these dilution factors on the distance will be discussed later in this Section. Note that the dilution factors depend on the bands used for temperature determination, thus, they are slightly different for T_{BVI} and T_{VI}.

Assuming spherically symmetric SN ejecta and homologous expansion, for each oberved epoch t, the distance D is given by the linear equation

$$t = t_0 + D\frac{\theta}{v_{ph}} \quad (6)$$

where t_0 is the moment of explosion, v_{ph} is the photospheric expansion velocity at epoch t. The velocities have been interpolated from the observed values listed in Table 7. The derived parameters relevant for the EPM analysis are listed in Table 9.

The EPM quantities are plotted in Fig. 16. The slope and the zero point of the fitted line gives the distance and the moment of explosion, respectively (see Eq.6). It is visible

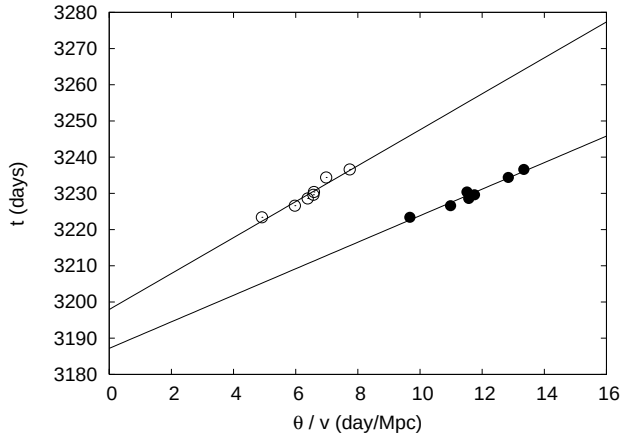

Figure 16. Distance determination in EPM via Eq.6. Parameters from T_{BVI} are plotted with filled circles, while those from T_{VI} are represented by open symbols. The fitted lines give the distance and the moment of explosion (see text).

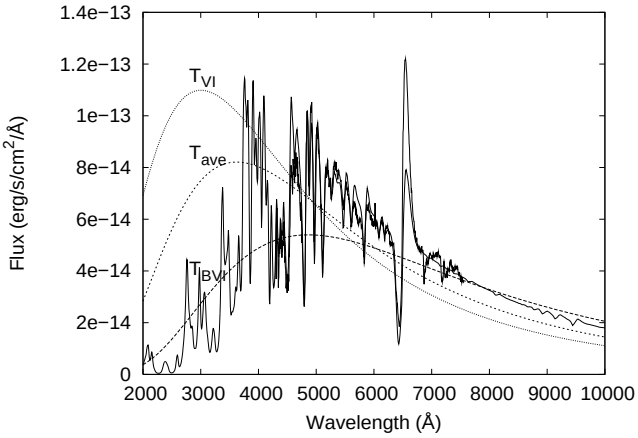

Figure 17. Flux distribution of blackbodies fitted in EPM, together with the observed and model spectrum on day +47 (Sect.3). The drop of flux in the blue region caused by metallic line blends (Fig. 14) and the continuum slope in the red cannot be fitted by a single blackbody. However, the total flux (but not its spectral distriution) may be adequately described by the blackbody with T_{BVI}.

Table 10. Results of EPM analysis. The uncertainties are given in parentheses. The quality of the fit (rms) is also shown.

Bands	t_0 (JD-2450000)	D (Mpc)	rms
BVI	3187 (3)	3.66 (0.3)	0.77
VI	3198 (4)	4.97 (0.6)	1.14

that the data from T_{BVI} and T_{VI} give quite different parameters, which is a usual situation in EPM (Leonard et al. 2002a,b).

Which solution is closer to the real one? The concept of EPM (diluted blackbody, spherical symmetry, etc.) received many criticism recently (Leonard et al. 2003; Baron et al. 2004), leading to a conclusion that EPM is at least "suspicious" and the results are systematically off from the real values. The discussion of all the problems is beyond the scope of this paper. Here we would like to show that combining the EPM results with those of other methods and the observations, it may be possible to select an EPM solution that is consistent with other results.

A critical step in EPM is the determination of the effective temperature, since it affects the calculated blackbody flux as well as the dilution factor. This quantity strongly depends on the selected wavelength bands (Table 9). Recently Dessart & Hillier (2005a) and Baron et al. (2004) showed that such kind of fitted blackbody temperature does not represent well the real spectral flux distribution of the SN atmosphere. Indeed, comparing the temperatures in Table 9 and the result of spectral modelling in Sect.3, it is clear that T_{BVI} is too low, while T_{VI} is too high with respect to the temperature (T_{bb} = 8000 K) that represents the spectrum observed on day +47 well. This is illustrated further in Fig. 17, where the observed spectrum and the *SYNOW* model computation are plotted together with blackbody flux distributions corresponding to T_{BVI} = 5955 K, T_{VI} = 9653 K and the average of these two temperatures. The blackbody curves were scaled according to the angular radius of the photosphere found by EPM.

It is clear that the continuum slope on the red side of the observed spectrum is indicative of higher temperature, but a blackbody with such a temperature fails to model the sudden drop of the flux below 4000 Å. Similar figures have been presented by Dessart & Hillier (2005a) and Baron et al. (2004) for SN 1999em. There is no doubt that the blackbody assumption is invalid, even in the very early phases (that were actually not observed in the case of SN 2004dj). The cause of this disagreement has been already shown in Fig. 14: the metallic line blends (especially the Ti II absorption) are responsible for the sudden decrease of the flux in the blue.

Fig. 17 shows that the blackbody with T_{BVI} has a flux distribution that does not give the best fit between 4000 and 6000 Å, but it adeqautely describes both the flux drop in the blue and the tail in the red. The two other curves that are closer to the real photospheric temperature have large excess flux below 4000 Å. These curves highly overestimate the photospheric flux in the blue bands, increasing the EPM distance. The T_{BVI} blackbody, however, results in a *bolometric* flux that is closer to the real bolometric luminosity, even though the spectral distribution is not perfectly matched. Since the purpose of EPM is to estimate the distance, rather than to model the spectra, the diluted blackbody assumption may be an acceptable compromise, if one regards it as the representation of the amount of integrated flux of the photosphere, rather than a physically correct model of the spectral flux distribution.

In principle, the application of a proper dilution factor should correct the flux for both the temperature mismatch between the SN and the blackbody, and the line blanketing. In this ideal case the same distance could be derived from any filter combinations. However, this is true only if the model spectrum (that was used to compute the dilution factor) perfectly fits the observed one. In reality, the metallic lines in the blue band can vary significantly from SN to

SN, which can be accounted for only with custom-crafted model atmospheres. This makes the usage of B band fluxes and temperature such as T_{BV} less effective for EPM.

Recently Dessart & Hillier (2005a) presented a new set of dilution factors appropriate for SNe IIp, that are systematically higher by 10 - 20 % than those given by Eastman, Schmidt & Kirshner (1996). In a follow-up paper Dessart & Hillier (2005b) showed that the application of their new dilution factors for SN 1999em increases its EPM-distance, bringing it into good agreement with the Cepheid-distance of the host galaxy, thus, eliminating most of the systematic errors of EPM found by Leonard et al. (2003). If one applies the dilution factors of Dessart & Hillier (2005a) for the present data of SN 2004dj, its EPM-distance will increase as $D_{BVI} = 4.3 \pm 0.3$ and $D_{VI} = 6.2 \pm 0.7$ Mpc. As in the case of SN 1999em, these distances are also systematically higher than those that were derived from the Eastman et al. dilution factors. The problem is that for SN 2004dj the EPM-distances are all *longer* than the values found by other methods (see below). In this case the application of the dilution factors of Dessart & Hillier (2005a) even increases the discrepancy between EPM and the other methods. It might be possible that the SNe IIp models by Eastman, Schmidt & Kirshner (1996) represents SN 2004dj better than SN 1999em, while the models applied by Dessart & Hillier (2005a) are better for SN 1999em. On the other hand, regarding the similarity of the optical spectra of these two SNe (Fig.10), it is hard to believe that the atmospheres are so different. Detailed modelling of the spectra of SN 2004dj may help to resolve this discrepancy.

Concluding the EPM analysis, we adopt the solution based on the Eastman et al. dilution factors and T_{BVI} (Table 10), namely $t_0 = 2453187 \pm 3$ and $D = 3.66 \pm 0.3$ Mpc as the moment of explosion and distance, respectively. In the followings we show that this distance is in agreement with other distance estimates for the host galaxy and SN 2004dj itself.

4.2 Standard Candle Method

The formulae for the SCM have been selected from Hamuy (2005) as follows:

$$V_{50} - A_V + 6.564 \log(\frac{v_{50}}{5000}) \; = \; 5 \log(H_0 \cdot D) - 1.478 \qquad (7)$$

$$I_{50} - A_I + 5.869 \log(\frac{v_{50}}{5000}) \; = \; 5 \log(H_0 \cdot D) - 1.926 \qquad (8)$$

where the observed quantities (V_{50}, I_{50}, v_{50}) are the V and I magnitudes and the radial velocity (in km/s) 50 days past explosion (i.e. in the middle of the plateau phase). Ideally, the distances obtained from the V and I data should be the same, therefore this method can also be used to test the consistency of the applied reddening correction.

From Table 3 and Table 6 we have chosen $V_{50} = 12.04 \pm 0.03$, $I_{50} = 11.40 \pm 0.03$ and $v_{50} = 3250 \pm 250$ km/s. The absorption corrections were computed from $E(B-V) = 0.07$ mag and the galactic reddening law, as before. For the Hubble constant $H_0 = 73$ km/s/Mpc has been adopted (Riess et al. 2005). This value is now based on both SNe Ia and Cepheid variables, and brings the previously conflicting distance scales into agreement. From these data we obtained $D_V = 3.47 \pm 0.2$ Mpc and $D_I = 3.52 \pm 0.2$ Mpc from the V and I calibration, respectively. The uncertainties are purely from the observational errors. These distances agree nicely with each other and with the EPM distance ($D_{EPM} = 3.66 \pm 0.3$ Mpc) within the errors, strengthening the credibility of both of the distance and reddening estimates.

Table 11. Comparison of distance estimates for SN 2004dj and NGC 2403.

Method	D (Mpc)	Reference
Tully-Fisher	3.50 ± 0.31	*LEDA*; Russell (2002)
Cepheid P-L	3.22 ± 0.15	Freedman et al. (2001)
EPM	3.66 ± 0.30	present paper
SCM	3.50 ± 0.20	present paper
average	3.47 ± 0.29	

4.3 Comparison with other distance determinations

The distances computed above are all based on the photometric and spectroscopic behaviour of the SN ejecta during the plateau phase. The overall uncertainty of such distances is about 20 % in the case of SCM (Hamuy & Pinto 2002), while it can be as large as 60 % for EPM (Leonard et al. 2003). Thus, the SN-distances should be compared with other distance estimates based on other methods, in order to test the possible systematic errors.

Since the host galaxy, NGC 2403, a member of the M81 group, is a nearby, well-studied object, its distance has been estimated from many other methods. These are listed in Table 11 together with the SN-based distances.

The Cepheid distance (Freedman et al. 2001) was usually applied in previous studies of SN 2004dj, but it is worth noting that this value is based on only I photometry without direct reddening determination. Freedman et al. (2001) *assumed* $A_I = 0.2$ mag as the I-band absorption during the distance measurement. From Table 11 it is visible that the SN-distances are in agreement with the recent Tully-Fisher distance, and differ less than 2σ from the Cepheid distance. This is not a significant difference, if one takes into account the additional uncertainty of the Cepheid distance due to the lack of reddening information. We conclude that the average distance of NGC 2403,

$$D \; = \; 3.47 \pm 0.29 \text{ Mpc}$$

is consistent with all available distance estimates within the errors.

5 PHYSICAL PARAMETERS

5.1 Nickel mass

During the tail phase the light curve is thought to be powered by radioactive decay of ^{56}Co - ^{56}Fe. Since ^{56}Co is the daughter nucleus of ^{56}Ni, the luminosity is proportional to the initial nickel mass produced by the explosion.

In order to estimate the nickel mass of SN 2004dj we compared the absolute bolometric light curve (calculated

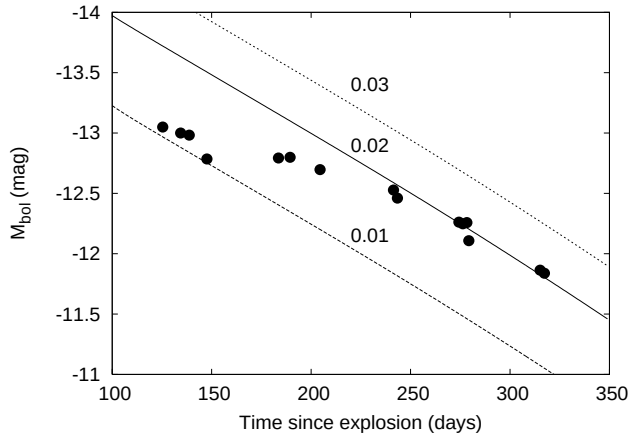

Figure 18. Comparison of absolute bolometric magnitudes of SN 2004dj (filled circles) with model computations (lines) during the early tail phase. Labels indicate the Ni-masses (in $M_\odot$).

from the "observed" $UVOIR$ bolometric light curve discussed in Sect.2.1.3, and the distance estimated in Sect.4) with the prediction of the simple light curve model described by Vinkó et al. (2004). This model calculates the luminosity in a homologously expanding SN ejecta, assuming radioactive decay, full gamma-ray and positron trapping and prompt thermalization of gamma photons and positrons. The density structure of the ejecta has been given as a power-law with exponent -7. This value is derived from the radius dependence of the optical depth $\tau(r) = \tau_0(r/R_{ph})^{-6}$ (found in Sect.4) by computing $\rho(r) = -\kappa^{-1}(d\tau/dr)$ and assuming spatially constant κ. The ejected mass has been set as $M_{ej} = 20M_\odot$ (see Sect. 5.2). The calculated light curves were mostly sensitive to the initial nickel mass, which was treated as a free parameter. Fig. 18 shows the light curves (thin lines) calculated with $M_{Ni} = 0.01,\ 0.02$ and $0.03\ M_\odot$. The observational data are also plotted for comparison as filled circles. Although during the observations SN 2004dj did not enter into the radioactive tail phase completely (the slope of the observed light curve differs from the calculated one given by the Co-decay), it is seen that the luminosity level can be explained with $M_{Ni} = 0.02 \pm 0.01\ M_\odot$. This nickel mass is the same as derived by Chugai et al. (2005) from the comparison of the absolute V light curves of SN 2004dj and SN 1987A. Based on the steepness of the V light curve measured after 100 days Kotak et al. (2005) got $M_{Ni} \sim 0.022\ M_\odot$.

Alternatively, the nickel mass can be determined using semi-empirical correlations, such as those presented by Elmhamdi et al. (2003a). Using their Eq.2 one can compute the nickel mass from the absolute V magnitude 35 days before the light curve inflection point. The moment of inflection point was found as $T_i = 2453297$ JD (Sect.2.1.1), and the absolute magnitude 35 days before that is $M_V(T_i - 35) = -15.52 \pm 0.1$ mag. The nickel mass is then $M_{Ni} = 0.022 \pm 0.002\ M_\odot$, in perfect agreement with the value derived above. From the steepness of the light curve during the transition phase Chugai et al. (2005) got $M_{Ni} = 0.013 \pm 0.004 M_\odot$. It is concluded that all the methods applied here agree that the estimated nickel mass of SN 2004dj is $M_{Ni} = 0.02 \pm 0.01\ M_\odot$. This is slightly below the nickel mass of SN 1999em and SN 1999gi (Elmhamdi et al. 2003a), which is an expected result based on the light curves (Sect.2.1.1).

Table 12. The adopted magnitudes for Sandage 96 (see Section 2.1 and Table 2).

Filter	λ (Å)	Mag.	Reference
U	3600	17.68	Larsen (1999)
B	4400	18.26	present paper
V	5500	17.85	present paper
R	7000	17.53	present paper
I	9000	17.06	present paper
J	12500	16.19	Sckrutskie et al. (1997)
H	16500	15.54	Sckrutskie et al. (1997)
K	22000	15.42	Sckrutskie et al. (1997)

5.2 Progenitor mass

Up to now the progenitors of Type II SNe have been identified directly in a number of cases (see Sect.1 for references). Surprisingly, these turned out to be relatively less massive stars, some of them being close to the theoretical limit of core collapse ($\sim 8M_\odot$). However, in most cases the progenitor could be detected only in a single bandpass, preventing the identification of its colour and evolutionary state.

SN 2004dj is particularly interesting in this respect, because its progenitor was a member of a compact cluster (Sandage 96) in NGC 2403. The age of a cluster can be determined more precisely than that of a single star, thus, the evolutionary state of the progenitor could be secured. Two groups have reported their observations of S96, made some years before the explosion (Maíz-Apellániz et al. 2004; Wang et al. 2005) and their analysis of the cluster SED (see Sect.1).

We have re-analysed the SED of S96 based on our own $BVRI$ photometry (Table 2) supplemented by data from the literature (Larsen 1999; Sckrutskie et al. 1997). Our optical photometry is in very good agreement with the observations published by Maíz-Apellániz et al. (2004), except for the $B-V$ colour index, where our value is closer to the one given by Chugai et al. (2005). The adopted magnitudes of S96 are shown in Table 12. Note that Maíz-Apellániz et al. (2004) reported a Gunn-Johnson color index $u - B = 0.41 \pm 0.06$ that differs from the $U - B = -0.51$ value given by Larsen (1999) in the Johnson system. We have preferred the latter value, since it is in the same photometric system as the other optical fluxes, but the U magnitude seems to be more uncertain than the fluxes in other bands. It may affect the derived cluster age, since it is connected with the amplitude of the Balmer-jump that increases with age.

We have selected two recent grids for calculating the model SEDs: the widely used model sequence by Bruzual & Charlot (2003) (BC03), based on Padova evolutionary tracks (that was also applied for S96 by Wang et al. (2005)), and a more recent one published by Jimenez et al. (2004) (J04), containing new stellar interior models, evolutionary tracks and improved treatment of mass loss. For the cluster initial mass function, a Salpeter IMF was adopted. It

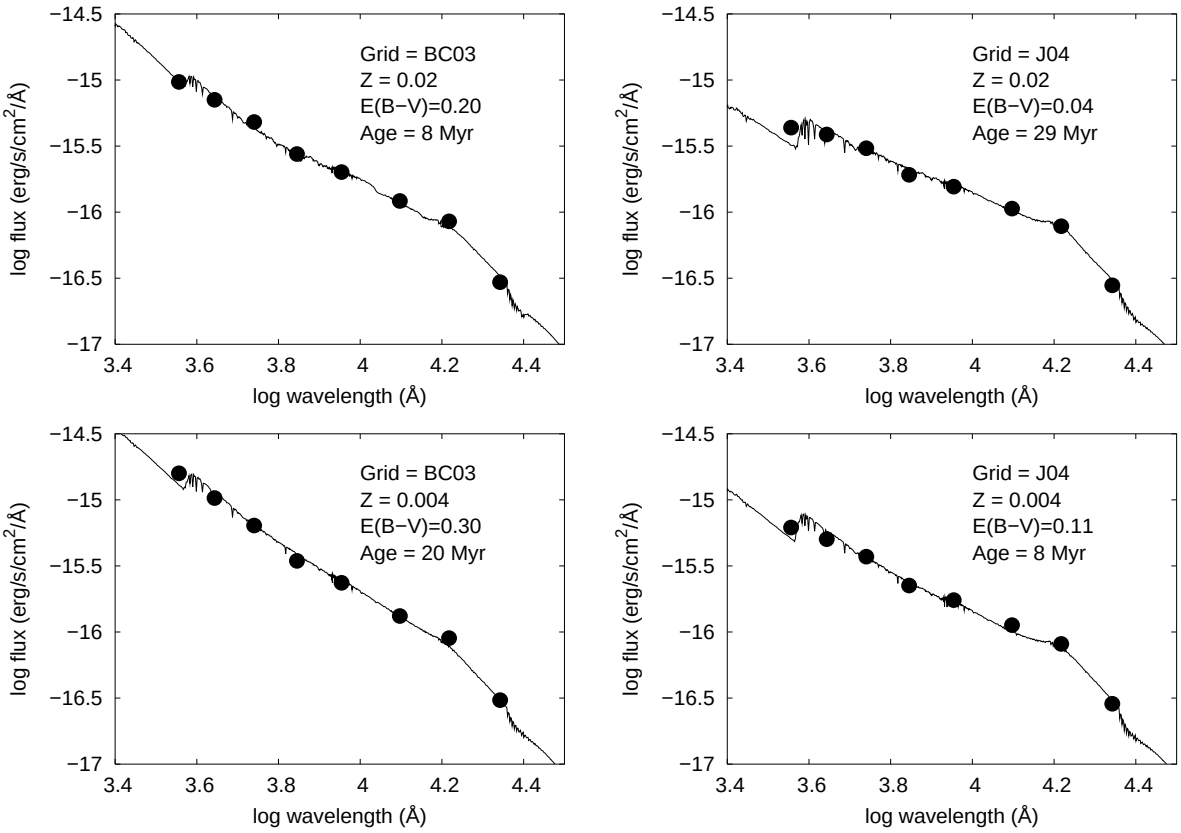

Figure 19. Results of SED fitting to the observed data of S96. The applied grids and the fitting parameters are indicated on each panel. See Table 13 for more information.

is known that the Salpeter function does not describe well the shape of the IMF, especially in the low mass regime. The selection of the Salpeter IMF was motivated mainly by the fact that the two previous studies for S96 also used this function, and we wanted to make the comparison of different solutions easier. For the same reason, a single starburst was assumed as the star formation history of S96.

The fitting has been computed via a simple χ^2 minimization. The observed magnitudes (Table 12) were transformed into monochromatic fluxes (in erg/s/cm^2/Å) using the calibration by Hamuy et al. (2001) (see Sect. 2.1.3), dereddened, and compared with the predictions of the spectral synthesis model grids. The fitted parameters were the cluster age T_{cl}, the cluster mass M_{cl} and the overall cluster reddening $E(B-V)_{cl}$. The metallicity of the cluster was kept fixed during the minimization. It should be noted that $E(B-V)_{cl}$ may be quite different from the reddening derived for SN 2004dj, because the compact cluster may contain a significant amount of intracluster gas and dust that is situated behind the SN. On the other hand, these parameters are correlated, and their simultaneous fitting may lead to spurious solutions. This is especially true for the reddening and the age, because a higher reddening correction would result in a bluer SED, indicating a lower age.

The resulting parameters corresponding to the minimum of χ^2 are listed in Table 13 and plotted in Fig. 19. Because the metallicity of NGC 2403 at the position of S96 is probably subsolar ([O/H] $= -0.24$, Pilyugin, Vilchez & Contini (2004); Wang et al. (2005)), we have used the models with $Z = 0.02$ and $Z = 0.004$ metallicities from both grids. Comparing these results with the published ones (shown in the last three rows of Table 13), it is visible that our analysis resulted in the same kinds of solutions as the previous studies: a "young" population with $T_{cl} = 8$ Myr and an "old" population with $20 < T_{cl} < 30$ Myr. The "old" solutions are very similar to the ones given in the previous studies. The "young" solution, however, has considerably less age. It is interesting that this solution comes out using both model grids, regardless of metallicity (but with different reddenings and cluster masses, of course). Based on the χ^2 values, the "young" solution from the BC03 grid gives the best description of the observed data. However, we agree with Wang et al. (2005) that if the observed SED is undersampled, such as the one presented here, it may be misleading to accept or reject solutions based on χ^2 values only. Thus, we conclude that, at present, there are three probable solutions for the SED fitting of S96: the old one corresponds to $20 < T_{cl} < 30$ Myr, the young one with $T_{cl} \approx 8$ Myr, and a solution with age between these two, $T_{cl} = 14$ Myr. Each solutions have their own combinations of cluster reddening and total mass, between the values of $0.04 < E(B-V) = 0.35$ and $30 < M_{cl} < 140 \cdot 10^3\ M_\odot$. Due to the correlations between these parameters, it is not possible to assign a unique solution for all these quantities simultaneously.

Regarding the potential progenitor of SN 2004dj, it is seen in Table 13 that the SN mass (determined from the Padova isochrones, Girardi et al. (1996)) ranges from

Table 13. Results of SED fitting for S96. The columns contain the followings: Model sequence, metallicity, cluster age (in Myr), cluster mass (in 10^3 $M_\odot$), cluster reddening (in mag), predicted SN mass for the given cluster age (in $M_\odot$, estimated from Padova isochrones), reduced χ^2 and reference. The last three rows list the solutions published by Maíz-Apellániz et al. (2004) and Wang et al. (2005).

Grid	Z	T_{cl} (Myr)	M_{cl} (10^3 $M_\odot$)	$E(B-V)_{cl}$ (mag)	M_{SN} ($M_\odot$)	χ^2	reference
BC03	0.02	8	38	0.20	24	0.47	present paper
J04	0.02	29	107	0.04	9.5	1.20	present paper
BC03	0.004	20	141	0.30	12	0.95	present paper
J04	0.004	8	29	0.11	26	0.96	present paper
SB99	0.02	14	24	0.13	15	0.16	Maíz-Apellániz et al. (2004)
SB99	0.02	29	57	0.23	9.5	1.58	Maíz-Apellániz et al. (2004)
BC03	0.008	20	96	0.35	12.5	0.77	Wang et al. (2005)

$\sim$ 10 $M_\odot$ to $\sim$ 25 $M_\odot$, depending on age. The uncertainty of the age determined from SED fitting is at least 10 % (Jimenez et al. 2004), implying an error of the SN-mass of about ± 4 $M_\odot$ for the young- and ± 1 $M_\odot$ for the old solution. It is interesting that the young (8 Myr) solution results in significantly higher mass than all the SNe IIp progenitor masses detected so far. The highest mass of a detected SN Type II progenitor is that of SN 1999ev (Maund & Smartt 2005) with 15 $M_\odot < M_{ZAMS} <$ 20 $M_\odot$. This is similar to the progenitor mass of SN 2004et, being $M_{ZAMS} = 15^{+5}_{-2}$ $M_\odot$ (Li et al. 2005a) and SN 1999gi with $M_{ZAMS} = 15^{+5}_{-3}$ $M_\odot$ (Leonard et al. 2002b). Contrary to these, the progenitors of SN 2003gd (Van Dyk et al. 2003; Smartt et al. 2004) and SN 2005cs (Li et al. 2005b; Maund, Smartt & Danziger 2005), also detected on pre-explosion images, are found within the mass range of $M_{ZAMS} = 7{-}9$ $M_\odot$. These two recent discoveries have led to a conclusion that perhaps all Type IIp SNe emerge from relatively less massive progenitors, so that $M_{ZAMS} = 8{-}15$ $M_\odot$. This is supported by the non-detection of the progenitors of SN 1999em, SN 1999gi and SN 2001du (Smartt et al. 2003) giving $M_{ZAMS} < 15$ $M_\odot$.

However, the possible masses of the progenitor of SN 2004dj determined above do not fully support this scenario. If the $T_{cl} = 8$ Myr solution of S96 is indeed valid, then the progenitor mass of SN 2004dj must have been higher than 20 $M_\odot$. This is significantly higher than the masses found for the other progenitors, even for SN 1999ev (see above). Since the other two solutions for S96 give progenitor masses that are consistent with the mass range of the others, it cannot be stated that SN 2004dj had definitely a more massive progenitor, but it cannot be ruled out at present. In principle, the cluster masses in Table 13 imply that there might be at least a few stars with $M > 20$ $M_\odot$ when SN 2004dj exploded. From the integration of the Salpeter IMF, the number of stars with $M > 20$ $M_\odot$ is $N(M > 20) \approx 2 \cdot (M/10^3 M_\odot)$, which gives $N(M > 20) = 58$ for $M_{cl} = 29 \cdot 10^3$ $M_\odot$. The actual number of massive stars in S96 may, of course, differ from this value, but statistically it is possible that at least a few such stars are indeed there. Maíz-Apellániz et al. (2004) estimated that S96 contains about 12 red and perhaps 2-3 blue supergiants, based on their SED parameters. The spectrophotometric observations of the remainder of S96 after the SN faded away would help to clarify the picture.

Comparing the observations of the CO vibrational bands in the mid-IR with theoretical explosion models combined with radiative transfer calculations, Kotak et al. (2005) presented evidence for a red supergiant with ~ 15 $M_\odot$ as the likely progenitor of SN 2004dj. Again, this is at the upper end of the detected progenitor masses for Type II SNe, close to the prediction of the ~ 14 Myr cluster solution by Maíz-Apellániz et al. (2004).

Zhang et al. (2005) estimated the parameters of the pre-supernova star using the formulae given by Nadyozhin (2003). These formulae relate the length of the plateau Δt_p, the middle-plateau absolute magnitude M_V and expansion velocity at the photosphere v_{ph} to the explosion energy (E_{exp}), ejected mass (M_{ej}) and progenitor radius (R). Zhang et al. (2005) derived $\Delta t_p = 80 \pm 21$ days, $M_V = -16.55 \pm 0.35$ mag and $v_{ph} = 3933 \pm 189$ kms^{-1}, and they got $E_{exp} = 0.75^{+0.56}_{-0.38} \times 10^{51}$ erg, $M_{ej} = 10^{+7}_{-5}$ $M_\odot$ and $R = 282^{+253}_{-122}$ $R_\odot$. From the more detailed analysis presented in this paper, we estimate these parameters as $\Delta t_p = 100 \pm 20$ days (Sect. 2.1.1, allowing $\delta t \approx 10$ days for the peak duration before the plateau, see Nadyozhin (2003)), $M_V = -15.88 \pm 0.18$ mag and $v_{ph} = 3250 \pm 250$ kms^{-1} (Sect. 4.2 and 4.3). These parameters result in $E_{exp} \approx 0.86^{+0.89}_{-0.49} \times 10^{51}$ erg, $M_{ej} \approx 19^{+20}_{-10}$ $M_\odot$ and $R \approx 155^{+150}_{-75}$ $R_\odot$. It is interesting that the ejected mass is, again, close to ~ 20 $M_\odot$, although with high uncertainty. It is concluded that the presently available information suggest that the progenitor mass of SN 2004dj is $M_{prog} \geq 15$ $M_\odot$. The SED fitting of S96 may suggest a cluster age as low as 8 Myr, indicating $M_{prog} > 20 M_\odot$. This massive progenitor may also be suspected from theoretical SN models.

6 CONCLUSIONS

The conclusions of this paper are summarized as follows:

- New $BVRI$ photometric observations of SN 2004dj are presented. The date of explosion is estimated as June 30, 2004 (JD 2453187$\pm$20), about 1 month before discovery. The plateau phase lasted about $\sim 110 \pm 20$ days after explosion. The most probable value of the reddening toward SN 2004dj is $E(B-V) = 0.07 \pm 0.1$ mag (Guenther & Klose 2004). The progenitor cluster S96 is also detected on pre-explosion frames.

• The new, plateau-phase optical spectra reveal great similarity between SN 2004dj and SN 1999em, a typical SN IIp. Radial velocities from metallic lines and $H\alpha$ are presented. The spectral features are successfully modeled with the spectrum synthesis code *SYNOW* with $T_{bb} = 8000$ K as the photospheric temperature. The observed P Cyg profile of $H\alpha$ can be better described by an increased emission of the photosphere relative to the blackbody intensity at the rest wavelength of $H\alpha$. A single nebular spectrum confirms the $H\alpha$ asymmetry reported by Chugai et al. (2005).

• The distance to SN 2004dj is estimated from two methods applicable for SNe IIp. The EPM distance is $D_{EPM} = 3.66\pm0.3$ Mpc, while the SCM gives $D_{SCM} = 3.50\pm0.2$ Mpc. These are in good agreement with other distance estimates to the host galaxy NGC 2403, based on Cepheids and TF-relation, although the Cepheid-distance is slightly less than the SN-distances. The averaged distance is $D = 3.47 \pm 0.3$ Mpc, which is consistent with all available information.

• Using the updated distance, the nickel mass of SN 2004dj is calculated as $M_{Ni} = 0.02 \pm 0.01\ M_{\odot}$ from the shape of the tail light curve. The progenitor mass has been estimated from fitting theoretical SEDs to the observations of S96. The solutions are similar to those of Maíz-Apellániz et al. (2004) and Wang et al. (2005), except that a "young" solution corresponding to $T_{cl} = 8$ Myr is also possible. Such a young cluster age would mean that the mass of the progenitor was $M > 20\ M_{\odot}$. The SN-masses of the other solutions are less than 15 $M_{\odot}$, being in better agreement with other SNe IIp progenitors.

ACKNOWLEDGMENTS

This research has been supported by Hungarian OTKA Grants No.TS 049872 and T042509. The authors are grateful to the directors and staff of Konkoly Observatory, Szeged Observatory (Hungary), David Dunlap Observatory (Canada) and F. L. Whipple Observatory (USA) for generously allocating telescope time. They also want to express their warm thanks to Prof. David Branch and his group members at University of Oklahoma for providing access and support to the SYNOW code. Thanks are also due to an anonymous referee for the very thorough report and numerous suggestions that helped us to improve the paper. The NASA Astrophysics Data System, the SIMBAD and NED databases, the Canadian Astronomy Data Centre and the Supernova Spectrum Archive (SUSPECT) were used to access data and references. The availability of these services are gratefully acknowledged.

REFERENCES

Adelman S.J. et al., 1989, A&AS 81, 221
Baron E., Hauschildt P.H., Branch D., 1994, ApJ 426, 334
Baron E. et al., 2000, ApJ 545, 444
Baron E., Nugent P.E., Branch D., Hauschildt P.H., 2004, ApJ 616, L91
Beswick R.J. et al. 2005, ApJ 623, L21
Branch D. et al. 2003, AJ 126, 1489
Branch, D. et al. 2004, ApJ 606, 413
Bruzual G, Charlot S., 2003, MNRAS 344, 1000
Chugai N.N. et al. 2005, Ast.L. 31, 792
Dessart L., Hillier D.J., 2005 A&A 439, 617
Dessart L., Hillier D.J., 2006, A&A 447, 691
Eastman R.G., Schmidt B.P., Kirshner R., 1996, ApJ 466, 911
Elmhamdi A., Chugai N.N., Danziger I.J., 2003, A&A 404, 1077
Elmhamdi A. et al. 2003, MNRAS 338, 939
Fisher, A. 2000, PhD Thesis, Univ. Oklahoma
Fraternali F., Oosterloo T, Sancisi R., van Moorsel G., 2001, ApJ 562, L47
Freedman W.L., Madore B.F., Gibson B.K. et al., 2001, ApJ 553, 47
Girardi L. et al., 1996, A&AS 117, 113
Guenther E.W., Klose S., 2004, IAU Circ. No. 8384
Hamuy M. et al., 2001, ApJ, 558, 615
Hamuy M., Pinto P.A., 2002, ApJ 566, L63
Hamuy, M. 2005, in Marciade J.M., Weiler K.W. eds., Proc. IAU Colloq. 192: Cosmic Explosions, On the 10th Anniversary of SN1993J, Springer Proceedings in Physics, p.535
Hendry, M.A., Smartt, S.J., Maund, J.R. et al., 2005, MNRAS 359, 906
Jimenez R. et al., 2004, MNRAS 349, 240
Kasen D., Branch D., Baron E., Jeffery D., 2002, ApJ 565, 380
Kharitonov A.V., Tereshchenko V.M., Kunyazeva L.N., 1988, in Spectrophotometric Catalogue of Stars (Alma-Ata, Nauka) p. 484
Kirshner R.P., Kwan J., 1974, ApJ 193, 27
Korcáková D. et al., 2005, IBVS No. 5605
Kotak R. et al., 2005, ApJ 628, L123
Larsen S.S., 1999 A&AS 139, 393
Leonard D.C. et al., 2002, PASP 114, 35
Leonard D.C. et al., 2002, AJ 124, 2490
Leonard D.C., Kanbur S.M., Ngeow C.C., Tanvir N.R., 2003, ApJ 594, 247
Li W., Van Dyk S.D., Filippenko A.V., Cuillandre J.-C., 2005, PASP 117, 121
Li W. et al. 2005, preprint (astro-ph/0507394)
Maíz-Apellániz J. et al., 2004, ApJ 615, L113
Maund J.R., Smartt S.J., 2005, MNRAS 360, 288
Maund J.R., Smartt S.J., Danziger I.J., 2005, MNRAS 364, 33
Nadyozhin D.K. 2003 MNRAS 346, 97
Nakano, S. et al. , 2004, IAU Circ. No. 8377
Patat F., Benetti S., Pastorello A., Filippenko A.V., 2004, IAU Circ. No. 8378
Phillips M.M., Williams R.E. 1991 in Woosley S.E. ed. Supernovae, Springer, N.Y., p. 36.
Pilyugin L.S., Vilchez J.M., Contini T., 2004, A&A 425, 849
Pooley D., Lewin W.H.G., 2004, IAU Circ. 8390
Riess A.G. et al., 2005, ApJ 627, 579
Russell D.G., 2002, ApJ 565, 681
Sárneczky K. et al., 2005 in Marciade J.M., Weiler K.W. eds., Proc. IAU Colloq. 192: Cosmic Explosions, On the 10th Anniversary of SN1993J, Springer Proceedings in Physics, CD-ROM
Schlegel D., Finkbeiner D., Davis M., 1998, ApJ 500, 525
Skrutskie M.F. et al 1997 in Garzón F. et al. eds, The Im-

pact of Large Scale Near-IR Sky Surveys, ASSL Vol.210, Kluwer, p.25
Smartt S.J. et al., 2003, MNRAS 343, 735
Smartt S.J. et al., 2004, Science 303, 499
Stockdale, C.J. et al., 2004, IAU Circ. 8379
Sugerman B., Van Dyk S., 2005, IAU Circ. No. 8489
Suntzeff N.B., 2000, American Institute of Physics Conference Series, 522, 65
Van Dyk S.D., Li W., Filippenko A.V., 2003 PASP 115, 1289
Vinkó, J. et al., 2004, A&A 427, 453
Wang, X. et al., 2005, ApJ 626, 89
Woosley S.E., Weaver T.A., 1986, Ann. Rev. Astron. Astroph. 24, 205
Yamaoka K., Maíz-Apellániz J., Bond H.E., Siegel M.H., 2004, IAU Circ. No. 8385
Zhang, T. et al., 2005, preprint (astro-ph/0512526)